








The Solar Neighborhood. XLIII. Discovery of New Nearby Stars with $\mu < 0''.18 \text{ yr}^{-1}$ (TINYMO Sample)

Adric R. Riedel¹ , Michele L. Silverstein² , Todd J. Henry³, Wei-Chun Jao² , Jennifer G. Winters⁴ , John P. Subasavage⁵ ,
Lison Malo⁶, and Nigel C. Hambly⁷

¹Space Telescope Science Institute, Baltimore, MD 21218, USA; riedel@stsci.edu

²Physics and Astronomy Department, Georgia State University, Atlanta, GA 30302, USA

³RECONS Institute, Chambersburg, PA, USA

⁴Harvard-Smithsonian Center for Astrophysics, Cambridge, MA 02138, USA

⁵US Naval Observatory Flagstaff Station, Flagstaff, AZ 86005, USA

⁶Canada–France–Hawaii Telescope, Kamuela, HI 96743, USA

⁷Institute for Astronomy, University of Edinburgh, Blackford Hill, Edinburgh, EH9 3HJ, Scotland, UK

Received 2018 April 23; accepted 2018 May 22; published 2018 July 12

Abstract

We have conducted a novel search of most of the southern sky for nearby red dwarfs having low proper motions, with specific emphasis on those with $\mu < 0''.18 \text{ yr}^{-1}$, the lower cutoff of Luyten’s classic proper-motion catalog. We used a tightly constrained search of the SuperCOSMOS database and a suite of photometric distance relations for photographic *BRI* and 2MASS *JHK*, magnitudes to estimate distances to more than 14 million red dwarf candidates. Here we discuss 29 stars in 26 systems estimated to be within 25 pc, all of which have $\mu < 0''.18 \text{ yr}^{-1}$, that we have investigated using milliarcsecond astrometry, *VRI* photometry, and low-resolution spectroscopy. In total, we present the first parallaxes of 20 star systems, 9 of which are within 25 pc. We have additionally identified 14 young M dwarfs, of which 3 are new members of the nearby young moving groups, and 72 new giants, including two new carbon stars. We also present the entire catalog of 1215 sources we have identified by this means.

Key words: astrometry – stars: distances – stars: low-mass – stars: pre-main sequence – surveys – techniques: spectroscopic

Supporting material: machine-readable table

1. Introduction

The solar neighborhood is the best laboratory for studying the Galaxy in which we live. The optimal place to make a volume-limited study of stars is nearby, where the very faintest stellar and substellar objects are easiest to detect and measure. Nearby binary systems are excellent targets for dynamical mass determination; they are resolvable with smaller orbits and shorter orbital periods than their more distant counterparts. Planetary-mass objects are brighter and have larger angular separations for the same linear separation when they are closer.

Most surveys to reveal the Sun’s nearest neighbors focus on detecting stars exhibiting high proper motions, μ . Such surveys identify two categories of stars: disk stars that are close enough that their modest Galactic orbital motion yields an apparent angular motion above the search threshold, and more distant stars with much higher intrinsic motions, e.g., subdwarfs and halo stars. This property of large proper motion has served nearby star research well from the very beginning, forming at least part of the decisions of Bessel (1838) and Henderson (1839) to observe 61 Cygni and Alpha Centauri (respectively) for the first parallaxes. These searches have continued on into the present day, encompassing everything from historical efforts like the Luyten Half Second catalog (Luyten 1957, 1979) to recent efforts like LSPM-North (Lépine & Shara 2005) and the Research Consortium On Nearby Stars (RECONS) group’s own work (e.g., Henry et al. 2004; Subasavage et al. 2005a, 2005b; Finch et al. 2007; Boyd et al. 2011a, 2011b). These searches have yielded thousands of stars that are candidates for stars within 25 pc, the horizon adopted by the Catalog of Nearby

Stars (Gliese & Jahreiß, 1991) and NStars (Backman et al. 2001) compendia.

Nearly all known nearby stars have high proper motions. An analysis of the current RECONS 10 pc sample⁸ to explore the realm of low- μ nearby stars is revealing. Of the 259 systems (not including the Sun) within 10 pc as of 2012 January 01, 133 (52%) have $\mu \geq 1''.00 \text{ yr}^{-1}$, 88 (35%) have $1''.00 \text{ yr}^{-1} > \mu \geq 0''.50 \text{ yr}^{-1}$, and 32 (13%) have $0''.50 \text{ yr}^{-1} > \mu \geq 0''.18 \text{ yr}^{-1}$. Only two stars, less than 1% of the total sample, have $\mu < 0''.18 \text{ yr}^{-1}$: GJ 566 AB (spectral type G8V, $V = 4.67$ (Høg et al. 2000), $\mu = 0''.169 \text{ yr}^{-1}$) and LSPM J0330+5413 (an M dwarf with $V \sim 16$, $\mu = 0''.150 \text{ yr}^{-1}$; Lépine & Shara 2005).

There are reasons to suspect that a small but significant population of nearby, very low-proper-motion stars have been overlooked. The limits of the proper-motion samples set above are based on historical precedent. In particular, the value of $0''.18 \text{ yr}^{-1}$ as the lowest interesting proper motion, used by RECONS’s other survey samples (e.g., Winters et al. 2017) as its lower limit, comes from the influential surveys of Luyten (Luyten Palomar, Luyten Bruce, Luyten Two Tenths, New Luyten Two Tenths) and Giclas (Southern survey). Those studies were themselves influenced by the work of the Royal Greenwich Observatory, particularly Thackeray (1917) and Dyson (1917), the latter of which suggests that Greenwich set their $0''.2 \text{ yr}^{-1}$ limit based on calculations that suggested only one-eighth of all nearby stars (<20 pc) should have lower

⁸ See Henry et al. (2006) for discussion of the definition of a RECONS 10 pc system and <http://www.recons.org> for updated statistics.

proper motions. Thus, from the outset, it was understood that some population of nearby stars would be overlooked.

In this paper, we present a survey of those very low-proper-motion stars, along with astrometric, photometric, and spectroscopic follow-up observations for selected high-priority stars and other additional targets of interest from the Cerro Tololo Inter-american Observatory Parallax Investigation (CTIOP) parallax program. In Section 2, we lay out the background work done on these “TINYMO” systems that have $\mu < 0''.18 \text{ yr}^{-1}$. In Section 3, we discuss the design and methodology of the TINYMO survey itself. In Section 4, we discuss further target characterization, which results in the final catalog of targets presented in Section 5. We then discuss the implications of the TINYMO survey in detail in Section 6 and the results of the observational follow-up of our targets in Section 7.

2. Expected Distribution of TINYMOs

A few surveys have delved into searches for stars with smaller proper motions, most notably Wroblewski–Torres–Costa (Wroblewski & Torres 1989 and subsequent; $0''.15 \text{ yr}^{-1}$), the LSPM survey (Lépine & Shara 2005; $0''.15 \text{ yr}^{-1}$), the “Meet the Cool Neighbors” group (Reid et al. 2007; limit $0''.11 \text{ yr}^{-1}$ northern hemisphere, $0''.28 \text{ yr}^{-1}$ southern hemisphere), Deacon & Hambly (2007; $0''.1 \text{ yr}^{-1}$), and Deacon et al. (2009; $0''.08 \text{ yr}^{-1}$). Apart from the anticipated but currently unreleased Lépine SUPERBLINK catalogs ($0''.04 \text{ yr}^{-1}$ and larger), no efforts are searching for stars with proper motions smaller than $0''.1 \text{ yr}^{-1}$ or down to truly zero proper motions. These comprehensive searches have not been done because, without the telltale marker of motion on photographic plates (or, more recently, CCD images), the investigator looking for nearby stars is inundated by huge numbers of candidates that come pouring out of automated searches (UCAC, Zacharias et al. 2013; PPMXL, Röser et al. 2011).

2.1. Incompleteness of the 25 pc Sample

How many stars do we expect to find within 25 pc at very low proper motions? For the purposes of this work, we have made an estimation, using a simulation of the solar neighborhood, accounting for spatial and velocity distributions. The spatial distribution within 25 pc is assumed to be uniform because the volume density of K stars (and hotter) in the RECONS 25 pc sample (W.-C. Jao et al. 2018, in preparation) is essentially uniform (Figure 1). The decreasing spatial distribution of M dwarfs is assumed to be the result of luminosity-related incompleteness. Accordingly, we assume the overall stellar density matches that of the nearest 5 pc (52 systems in 5 pc, or $0.099 \text{ systems pc}^{-3}$) and expect 6500 systems within 25 pc. (Note that Regulus is the sole known B star within 25 pc and not within that 5 pc radius.) The velocity distribution of the solar neighborhood is modeled according to the spectral type of the stars, as given in Aumer & Binney (2009). The hottest stars have the lowest dispersions around the local standard of rest, and cooler stars have increasingly large velocity dispersions up until the Parenago discontinuity around $B - V = +0.9$, where the average stellar population has had uniform amounts of disk heating. Additional kinematic parameters for subdwarfs and white dwarfs are sourced from Gizis (1997) and Mihalas & Binney (1981), respectively.

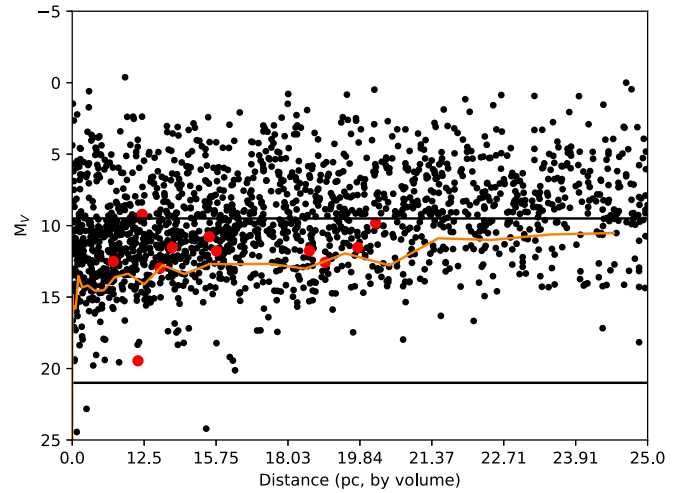


Figure 1. Absolute V magnitude vs. distance for stars within 25 pc, from the RECONS 25 pc database (W.-C. Jao et al. 2018, in preparation). The distance is given in equal-volume elements to properly represent stellar density. The density is essentially uniform for stars brighter than $M_V = 9$, suggesting completeness for A, F, G, and K stars; 90% of stars lie above the orange line, demonstrating that completeness decreases at larger distances. Red dots represent the 11 systems within 25 pc with new parallaxes in this paper.

Table 1
Parameters for Synthetic 25 pc Sample

$V - K_s$	Cum. Frac.	σU km s $^{-1}$	σV km s $^{-1}$	σW km s $^{-1}$	Note
-1	0.0000	8	8	5	B systems (Regulus = 1/6375)
0	0.00016	14	9	4.5	A systems (4/408)
1	0.0098	22	14	10	F systems (6/408)
2	0.0245	38	26	20	G systems (20/408)
3	0.0735	37	26	19	K systems (44/408)
3.8	0.1814	37	26	19	M0-3 systems
5	0.3500	37	26	19	M3-5 systems
6	0.5000	37	26	19	M5-7 systems
8	0.7200	37	26	19	M7-9.5 systems
10	0.8100	37	26	19	L, T systems
20	0.91186	37	26	19	Transition ^a
-1	0.91187	177	100	82	Subdwarfs ^b
20	0.92336	177	100	82	Transition ^a
-1	0.92337	50	30	20	White dwarfs ^c
0	0.9500	50	30	20	White dwarfs
2.7	1.0000	50	30	20	White dwarfs

Notes. The cumulative luminosity function distribution of stars is in three sequences—main sequence, subdwarfs, and white dwarfs—used to randomly generate a proportional and representative 25 pc sample.

^a These are not real; they are a computational necessity included to separate the “sequences” and prevent interpolation from making many oddly distributed stars from a continuous function.

^b Gizis (1997).

^c Mihalas & Binney (1981).

To tie the spherical and velocity distributions together, we used the color distribution of spectral types in the RECONS 25 pc database (together with the assumption that all of the missing star

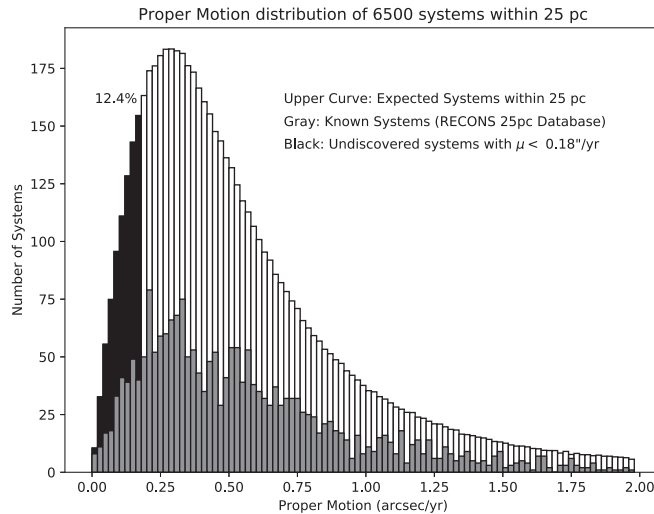


Figure 2. Simulated proper-motion distribution using Mihalas & Binney (1981), Gizis (1997), and Aumer & Binney (2009) velocity distributions and a cumulative mass function from RECONS data. The top black-and-white plotted histogram assumes 6500 star systems within 25 pc, based on the assumption that 52 systems within 5 pc is a representative spatial density. Systems moving slower than $0''.18 \text{ yr}^{-1}$ are noted in black; the gray curve represents actual proper motions from the RECONS 25 pc sample (W.-C. Jao et al. 2018, in preparation).

systems would be K, M, L, or T dwarfs with the same velocity dispersion) and generated a cumulative luminosity distribution (Table 1) out of which a random number generator can provide appropriately distributed stars of different spectral types, luminosities, and dispersions. These randomly generated stars were placed in a uniform spatial distribution with a radius of 25 pc. Strömberg’s asymmetric drift equation ($\langle V \rangle = \frac{U^2}{k}$, $k = 74 \pm 5$; Aumer & Binney 2009) was added to the stars, and the UVW velocity of the Sun relative to the local standard of rest ($U = 11.10$, $V = 12.24$, $W = 7.25 \text{ km s}^{-1}$; Schönrich et al. 2010) was subtracted. We then derived the observational properties (R.A., decl., proper motion, radial velocity) from these synthetic stars. The distribution of proper motions, as derived from 10 million synthetic stars, is shown in Figure 2.

As can be seen in Figure 2, the RECONS 25 pc sample is incomplete for all proper motions but particularly for proper motions less than $0''.5 \text{ yr}^{-1}$, with peaks in both around $0''.3 \text{ yr}^{-1}$. Overall, 12.4% of all stars within 25 pc should be moving at speeds slower than $0''.18 \text{ yr}^{-1}$, which is in line with other estimates (Reid et al. 2007, for example, found 11%).

There are potential improvements to this simulation. No giants, young stars, or any of the local kinematic streams (as seen in Skuljan et al. 1999; Nordström et al. 2004) were included in this analysis. An additional possible improvement would be to model stars as bursts of star formation with a cluster mass, IMF distribution, and age-associated velocity dispersion.

3. The TINYMO Survey

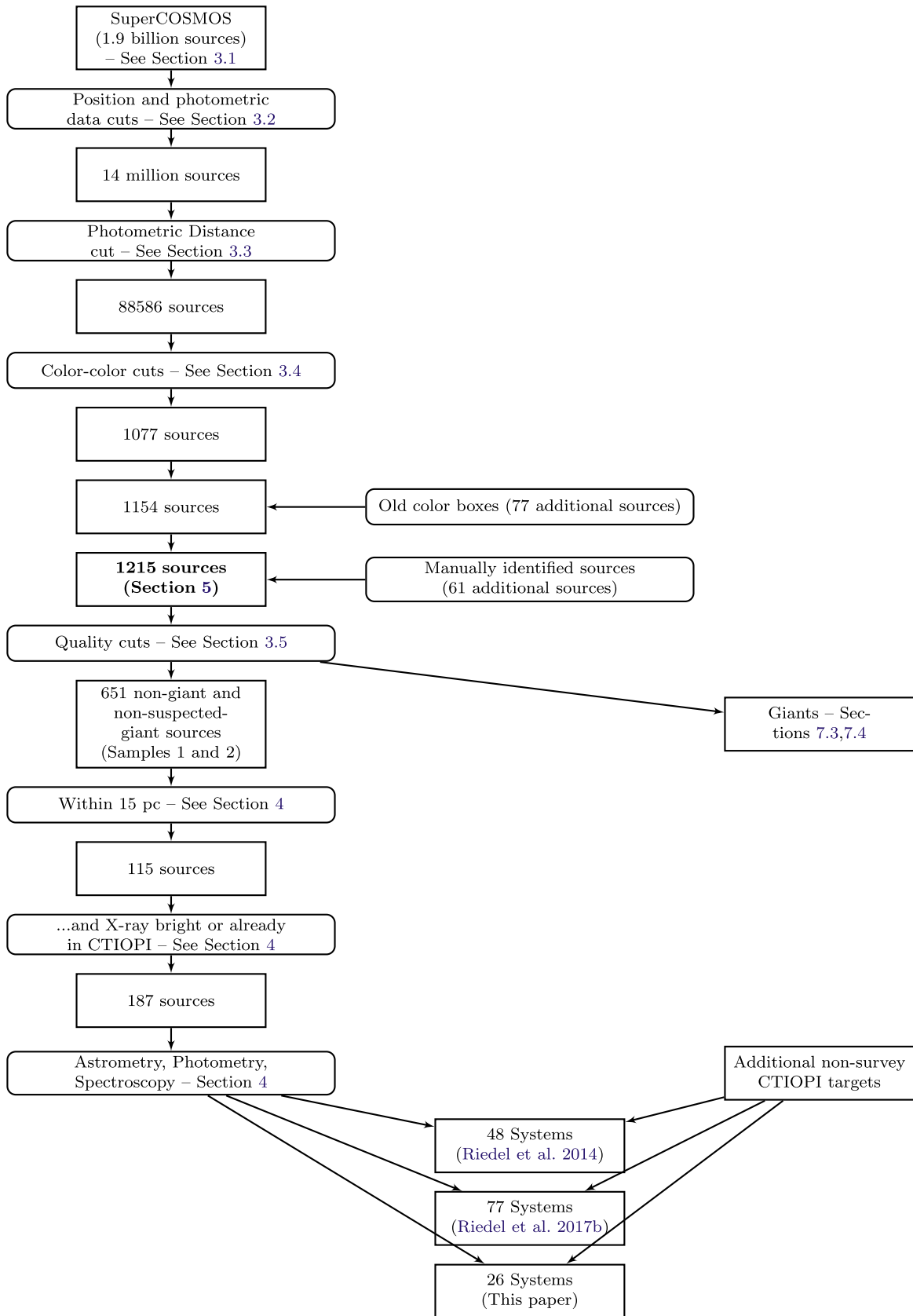
To create a more detailed picture of the solar neighborhood, we have carried out a search of the southern sky for stars with tiny proper motions, less than $0''.18 \text{ yr}^{-1}$, dubbed TINYMO. This is a regime of proper motions that has not been explored in a rigorous way. The discoveries reported here complement

previous SuperCOSMOS-RECONS (SCR) searches of the southern sky (Hambly et al. 2004; Henry et al. 2004; Subasavage et al. 2005a, 2005b; Finch et al. 2007; Boyd et al. 2011a, 2011b); in particular, the last three revealed 6007 new proper systems with $0''.40 \text{ yr}^{-1} > \mu \geq 0''.18 \text{ yr}^{-1}$ between declinations -90° and -00° , and $R_{59F} = < 18.0$.

Those previous searches used proper-motion cuts to identify potential nearby stars, followed by photometric estimates of distance to pick the most promising nearby young objects for astrometric and spectroscopic follow-up through the CTIOPI. The search discussed here is almost entirely the opposite of those searches, starting with a rough proper-motion limit and then using photometry to select the promising nearby stars. Photometry is rarely the primary method of identifying nearby stars (one of the rare other examples is Cruz et al. 2007, which identified late-type red and brown dwarfs by their extreme colors) because of the enormous contamination of distant giants and other non-nearby sources.

Despite this challenge, a photometric search is the only way to reliably identify genuinely nearby tiny proper-motion stars. Even allowing for the practical limitations of proper-motion measurements (particularly those of compiled catalogs, which have uncertainties introduced by source/scanning resolution and optical defects), below a certain level (see Section 6.3), even distant background stars have some nonzero proper motion because they too are in orbit around the Galactic center.

In this paper, we estimate distances en masse for millions of sources, then target those with the smallest distances for further consideration. The list of selected nearby red dwarf candidates is sequentially winnowed with quality and color cuts until only the most promising targets remain, and these are investigated individually for available data in the literature and targeted in observational programs (see Figure 3).



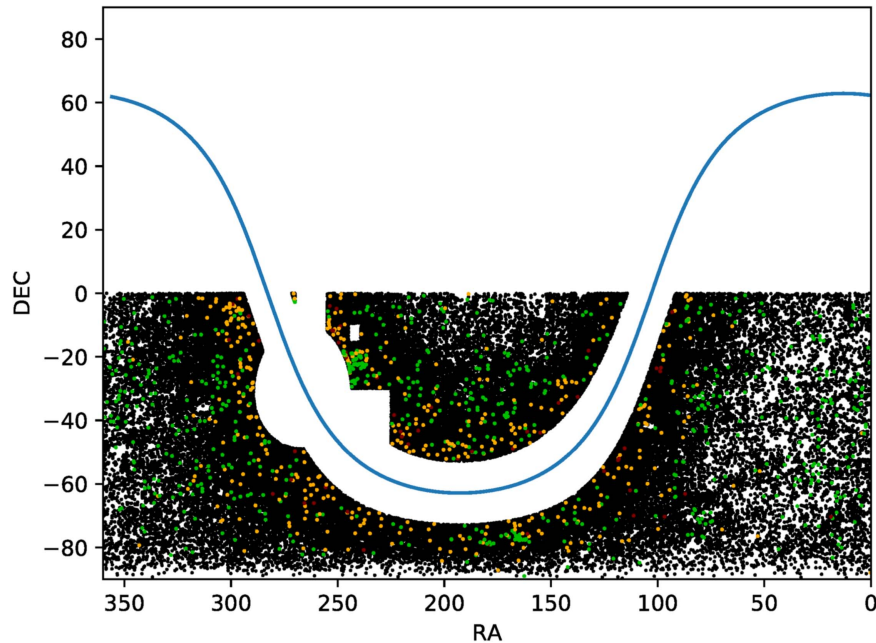


Figure 3. Sky map of the TINYMO survey extraction centered on R.A. = 0 hr, decl. = 0°, with a 10° band around the Galactic equator and a 20° region around the Galactic center removed, along with two regions near the north Galactic spur. The colored points (green = high-probability M dwarfs, yellow = lower-probability M dwarfs, red = probable giants) are stars selected by later phases of the survey processing (see Figure 4), demonstrating the crowding of sources around the Galactic bulge. The resulting sky coverage is roughly 16,000 deg², or 39.3% of the total sky, and contains just under 14 million targets that satisfy our photometric quality criteria.

3.1. SuperCOSMOS (1.9 Billion Sources)

SuperCOSMOS was a machine that scanned glass photographic plates for more than a decade at the Royal Observatory in Edinburgh (ROE), Scotland. The SuperCOSMOS Science Archive (SSA) database (Hambly et al. 2001b) is built from scans the machine made of primarily Palomar Observatory Sky Survey (POSS) and Science and Engineering Research Council (SERC) sky survey plates. The survey covers the entire sky at four different epochs and in four different passbands, deriving positions, proper motions, and (up to) four-color photometry for 1.9 billion sources. SuperCOSMOS magnitude limits vary by field but are generally equivalent to $B = 22$, $R = 20$, $I = 19$ in the plate photographic magnitude system of, e.g., Bessell (1986). The 2MASS JHK_s photometry has been cross-matched to sources where available. SuperCOSMOS is not a source of absolute positions or proper motions, though attempts were made to force the mean Galaxy proper motions (field by field) to zero in fields where galaxies were available (Hambly et al. 2001a). The overall reference frame was shifted to ICRS via cross-matching with 2MASS (which is linked to TYCHO-2).

Of interest to TINYMO, the plates were aligned by cross-matching stars out to distances of 6'' (in a spiral search pattern) between two plates. This matching constraint actually provides a variable upper limit on measurable proper motions. For the southern hemisphere, where epoch spreads are 30–40 yr, the maximum proper motion detectable is around 0''2–0''3 yr⁻¹, above which an object would move more than 6'' in that time. This represents a trade-off: a few higher-proper-motion stars—perhaps 100,000 out of two billion—will be identified as multiple transient objects. Previous RECONS proper-motion searches have been carried out using additional software designed to match up otherwise unmatched sources in the SSA. Other surveys using the SuperCOSMOS database (and their

own special software) include Scholz & Meusinger (2002 and subsequent), the Liverpool–Edinburgh High Proper Motion Survey (Pokorny et al. 2003), and the Southern Infrared Proper Motion Survey (Deacon et al. 2005).

For the purposes of TINYMO, the main catalog is sufficient, provided we limit ourselves to sources identified on all four plates. The catalog contains proper motions up to 0''3 yr⁻¹ for sources of interest, except in regions north of decl. = -18°, where far older POSS-I E red plates were used. In those areas, the larger epoch spread means that the highest proper motion that can be reliably extracted from the 6'' cross-match is roughly 0''12 yr⁻¹; it is also incomplete for a 25 deg² region around R.A. = 16 hr, decl. = -12° where POSS-I E field 1038 is missing (and thus no four-color detections are possible).

3.2. SQL Query (14 Million Sources)

The initial sift of the TINYMO survey was an SQL query, meant to identify meaningful targets in the southern hemisphere. To avoid overloading the server, the queries were conducted in tiles of R.A. and decl. The selection criteria were as follows.

3.2.1. Location Cuts

1. Regions in the southern hemisphere.
2. More than 20° from the Galactic center.
3. More than 10° from the Galactic plane.

These positional cuts were designed to limit the survey to the southern hemisphere and remove extremely dense areas (full of highly reddened stars that would contaminate the sample) from consideration. After the fact, additional cuts were made to the extracted data to remove regions near the north Galactic spur: $15 \text{ hr} \leq \text{R.A.} \leq 16 \text{ hr}$, $-30 \leq \text{decl.} \leq +00$; $15 \text{ hr} \leq$

R.A. ≤ 16 hr, $-60 \leq \text{decl.} \leq -30$; $17 \text{ hr} \leq \text{R.A.} \leq 18 \text{ hr}$, $-30 \leq \text{decl.} \leq +00$. Within those regions, there were as many stars with apparent photometric distances within 25 pc, all most likely giants at far greater distances, as there were in the rest of the sample (see Figure 3). The Large and Small Magellanic Cloud regions were not removed. This cut defines our coverage of 16,214 deg², or 39.3% of the sky.

3.2.2. Plate Detection Cuts

1. Detected on all four plates.

This criterion sets an upper proper-motion limit as described above, as well as limits on color; the star could not be so red that it did not appear in the B_J plate, which cuts out a number of cool and faint stars. As mentioned earlier, this also cut out a small region of sky (roughly $16 \text{ hr} \leq \text{R.A.} \leq 16:20$, $-15 \leq \text{decl.} \leq -10$) where there is no R_1 plate.

3.2.3. Quality Cuts

- Internal quality measure >128 on all plates.
- Ellipticity less than 0.2 on all plates.

These cuts removed a large number of extragalactic sources, unresolved binaries, and spurious sources, including plate defects.

3.2.4. Luminosity Cuts

1. Brighter than $R_2 = 16.5$.

The R_2 magnitude limit allows for detection of stars with $B_J = 21$ and $B_J - R_2$ colors as red as 4.5 (a brown dwarf) and matches the Giclas surveys (Giclas et al. 1979), as well as previous SCR proper-motion surveys, not including Boyd et al. (2011a).

3.2.5. Offset Cuts

1. Detected in 2MASS within 5" of the weighted mean plate position.

The mean plate position recorded by SuperCOSMOS is weighted by the positional accuracy of each of the detections; the epoch of this effective plate position is usually around 1985, while the mean epoch of 2MASS is around 2000. Thus, any star moving slower than $\mu < 0''.333 \text{ yr}^{-1}$ (less than $\sim 5''$ motion over 15 yr) will be matched to its 2MASS entry. This, in concert with the four-plate detection requirement, makes the most stringent cut.

The photometric limits chosen influence the kinds of stars we expect to find. The limit of 2MASS is effectively $JHK \approx 15$. SuperCOSMOS contains sources as faint as $B_J = 21$, so with a magnitude cutoff of $R_2 = 16.5$, the limiting magnitudes for M dwarfs are all therefore set by the R_2 filter. The magnitudes of an M0V star ($M_{B_J} = 10$, $B_J - R_2 = 2.3$, $B_J - K = 4.5$) corresponding to our cutoff at $R_2 = 16.5$ are $B_J = 18.8$, $R_2 = 16.5$, and $K = 14.3$. This implies a limiting distance of 630 pc. For an M9.0V star ($M_{B_J} = 20.4$, $B_J - R_2 = 3.0$, $B_J - K = 10.2$), the magnitude limit is $B_J = 19.5$, $R_2 = 16.5$, and $K = 9.3$, which implies a limiting distance of 6.6 pc. Within 25 pc, we should be able to detect every M dwarf bluer than $B_J - R_2 = 2.6$ (M7V).

Ultimately, the search identified just short of 14 million stars in the covered 16,214 deg² region seen in Figure 3.

3.3. Photometric Sift (88,586 Sources)

The next phase of the search for low-proper-motion nearby stars was the computation of photometric distance estimates (Hambly et al. 2004) for all stars. This method uses the plate BR_2I and 2MASS JHK colors to produce up to 11 distance estimates (out of a total possible 15 colors; $B - R_2$, $J - H$, $J - K$, and $H - K$ do not provide useful discriminants for red dwarfs) that are then combined into a weighted mean with a typical uncertainty of 26%. These color-magnitude relationships, described by fourth-order fits to the main sequence, are only valid for K and M dwarfs, which removes all hotter stars from our consideration. We expect that no stars hotter than K remain undiscovered within 25 pc thanks to the work of *Hipparcos*. Of the 14 million point sources from the first step, slightly fewer than 89,000 (see Figure 3) were estimated to be within 25 pc by those relations.

As there are only roughly 6,500 systems expected within 25 pc (Section 2.1), the $\approx 89,000$ figure suggests massive contamination. This is as expected: apart from subdwarfs and (theoretically) stars with unresolved white dwarf companions, contaminants with the colors of main-sequence stars are much brighter objects that will land in a magnitude-limited survey such as ours and include

- giants that mimic main-sequence colors or were caught at fortuitous times in their light curves, particularly Mira variables due to their intrinsic luminosity;
- metal-rich stars just beyond 25 pc;
- unresolved multiple stars, where there is extra luminosity and therefore a smaller expected distance;
- pre-main-sequence stars, where the extra luminosity is due to the enlarged radius of the gravitationally contracting protostar;
- reddened (and extincted) objects in molecular cloud regions; and
- redshifted active galactic nuclei.

The 11 plate relations were calibrated to colors typical of K and M main-sequence stars; if a star has unusual colors outside the valid color ranges, it is less likely to be a main-sequence star. We therefore flagged all objects with fewer than nine valid distance relations (out of 11 total). It should be noted that this limit is different from that used in other publications in this series, where as few as seven relations were accepted to accommodate the possibility that a single B_J or R_2 filter magnitude might be erroneous.

3.4. Color-color Cuts (1154 Sources)

To identify specifically main-sequence stars, we applied a color-color cut in $J - K$ versus $v - K$ space, where v is an estimated V magnitude formed by taking the average of B and R_2 .

There are, among the BR_2IJK color combinations, two particular colors in which M dwarfs are distinguishable from red giants: $J - H$ and $J - K$ (Figure 4). In these colors (and only these), mid-M dwarfs are bluer than mid-M giants of the same $v - K$ color. This property does not appear in any other combination of colors, including $H - K$, but it shows up when

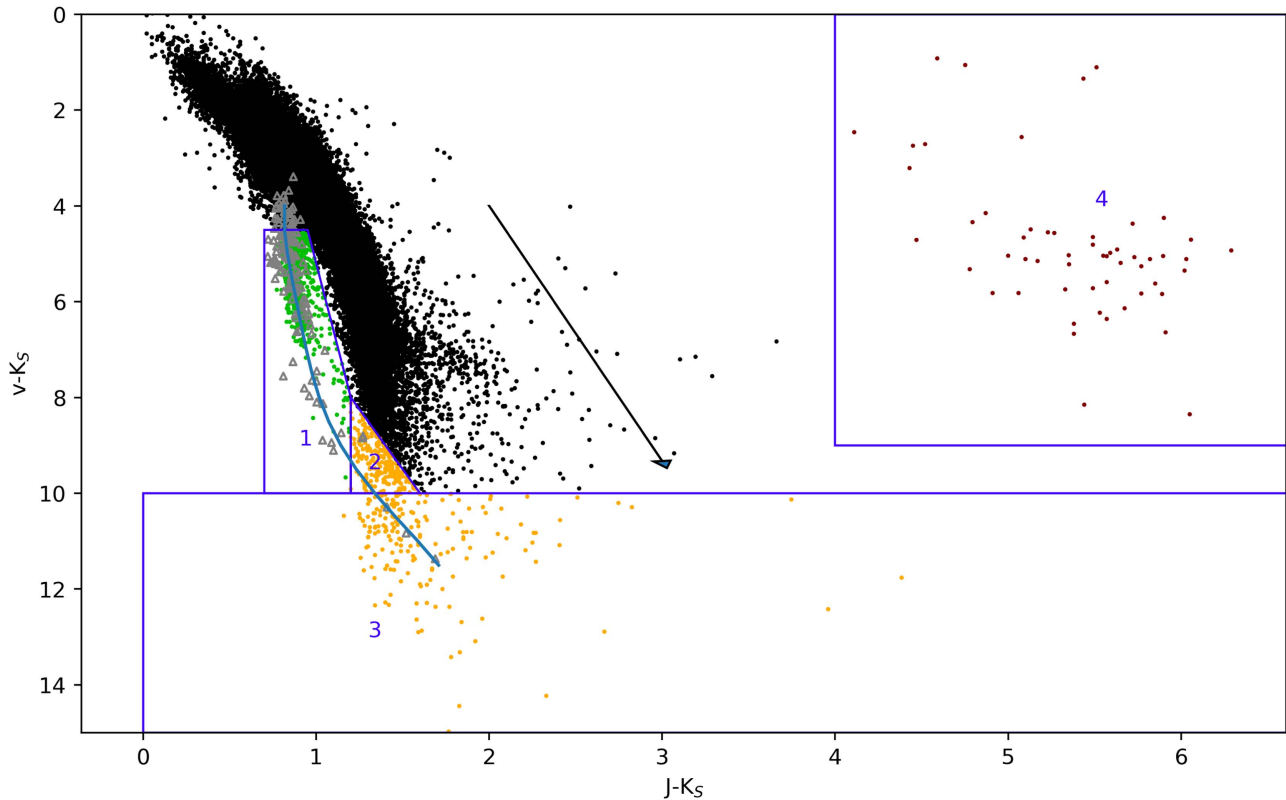


Figure 4. Using the color-color regions shown on this $J - K$ vs. $v - K$ diagram, we separate the 88,586 stars in Figure 3 into giants (black), dwarfs (green), and interesting overlap regions (yellow). The curve is a fifth-order fit to the main sequence (as determined by the RECONS 10 pc sample, plotted as gray triangles). The cluster of red points beyond $J - K = 4$ (“flyers”) were later revealed to be accidental cross-matches to spurious 2MASS entries. The selection boxes from Table 2 and Section 3.4 are shown here. The appropriate interstellar reddening vector from Fitzpatrick (1999; assuming $v, J, K_s =$ Johnson V, J, K) is also shown. Colors are the same as in Figure 3.

$J - H$ or $J - K$ is plotted against any other color. This behavior is most likely due to gravity-sensitive absorption features in all three bands: the J -band feature decreases in strength as gravity increases, and the H - and K -band features both increase in strength as gravity increases. Allers et al. (2007) identified a number of potentially gravity-sensitive features that may fit those requirements: VO and TiO weaken with increasing gravity (and are predominantly found in the J band), and CO (which dominates in the K band), KI, and Na I all strengthen with increasing gravity. This would explain why dwarfs are bluer in $J - H$ and $J - K$ (increased J flux, decreased H or K flux) and yet there is no effect on $H - K$ (correlated loss of flux). This behavior does not appear in other Johnson/Kron-Cousins/2MASS filter combinations, though R and I are also dominated by TiO; it may have to do with the rate at which the band strengths change.

Plotting the $J - K$ versus $v - K$ combination of colors (Figure 4) demonstrates a region of color-color space where M dwarfs are distinguishable from M giants entirely by photometric colors. To take advantage of that property, we have created four selection regions to separate out the data, as shown in Figure 4 and Table 2.

Region 1: Red Dwarf Candidates

In the red dwarf region, the main sequence is clearly separated from the giants, as seen in Figure 4. This is the most reliable region for nearby star detections using our search technique and encompasses spectral types M3.0V through M9.0V. The region has been drawn with a blue cutoff of $v - K = 4.50$ to avoid the broad sequence of giants with bluer

Table 2
The TINYMO Color Selection Regions

Box	Vertices		Purpose
	$J - K$	$v - K$	
1	0.7	4.5	Main sequence
	0.95	4.5	
	1.2	8.0	
	1.2	10.0	
	0.7	10.0	
2	1.2	8.0	Brown dwarfs
	1.6	10.0	
	1.2	10.0	
3	0.0	10.0	Very red dwarfs
	7.0	10.0	
	7.0	15.0	
	0.0	15.0	
4	4.0	0.0	“Flyers”
	7.0	0.0	
	7.0	9.0	
	4.0	9.0	

$v - K$ seen above the dwarfs, although some nearby stars should be found in this region. Some giants will still bleed into Region 1 near the $J - K = 0.95$, $v - K = 4.50$ corner; the amount of contamination varies from field to field and appears to be related to the Galactic latitude of the region and its

particular reddening. The red edge of the sample is cut at $J - K = 1.2$, beyond which the giant and brown dwarf colors overlap.

Region 2: Giants' Tail

The tail of the giant sequence crosses the dwarf sequence in Region 2, but we have retained these targets because one or more may be a very nearby late-type red or brown dwarf.

Region 3: Very Red Candidates

Region 3 includes extremely red objects ($v - K > 10$) that are also likely giants or highly reddened distant stars but could be interesting unusually red sources.

Region 4: Flyers

A small group of extremely red sources (called “flyers”) were found to have $v - K = 0-7$ and $J - K = 4-7$. Investigation showed that all were bright targets on the SuperCOSMOS plates, with erroneous matches to 2MASS sources. All checked objects were later determined to be giants falling within the giant locus once their photometry was corrected.

The result of accepting only the objects in these four regions was a reduction of 88,586 candidates to 1077 promising nearby objects. An early selection attempt used different boxes that included 77 stars⁹ not in the final set of boxes (see Figure 3), which we retain in our final catalog for bookkeeping reasons. This brings the total to 1154 stars.

3.5. Further Quality Cuts

In the fourth and final phase of the winnowing, more quality cuts were made to improve the nearby star recovery rate.

1. Visual inspection (“blinking”) of SuperCOSMOS plate scans in the Aladin Skyview Desktop applet with the 2MASS Point Source Catalog loaded as an overlay to ensure detected stars were (a) real objects, (b) moving (proper motions larger than $0''.08 \text{ yr}^{-1}$ were identifiable under visual examination), and (c) matched to the proper 2MASS point (mistakes in the 2MASS identification account for the “flyers” mentioned in Section 3.4). At this point, an additional 61 proper-motion objects (generally companions) were nonexhaustively identified by eye to bring the total candidate list to 1215 objects.
2. Comparisons of the two R -band SuperCOSMOS magnitudes for consistency. Values differing by more than 1.00 mag were likely variable giants and were discarded. This is admittedly imperfect: low-amplitude Mira variables or Miras caught at two similar points in their light curve will not be flagged by their $R_1 - R_2$ magnitudes, while stars with bad R_1 or R_2 photometry will be unfairly excluded.
3. Elimination of sources with $J - K \geq 2.00$, which are presumed giants or stars with poor JHK magnitudes that corrupt the distance estimates.
4. Searches of the SIMBAD database to determine whether or not sources are previously documented nearby stars, giants, Mira stars, carbon stars, and/or pulsating or variable stars.
5. Searches of the *ROSAT* All-Sky Survey (RASS) bright source (Voges et al. 1999) and faint source (Voges et al. 2000) catalogs for stars with X-ray detections, which are most likely dwarfs or young stars.

⁹ None of the 77 objects show signs of being main-sequence stars.

We thus arrive at a sample of 651 stars that pass all tests, while the remaining 564 of the 1215 objects were flagged for any number of the above quality reasons.

We developed five classifications for stars based on the above quality cuts, which we use to reclassify the sources identified in the four-color boxes defined above and will refer to from this point on as follows.

1. X-ray: Stars that had X-ray counterparts in the RASS-BSC and RASS-FSC catalogs were highest priority, as they were most likely to be nearby dwarfs.
2. Good: Stars that passed all quality cuts but did not have X-ray detections.
3. Probable: Stars that either failed the $R_1 - R_2$ test, had fewer than nine valid photometric plate distance relations, or $J - K \geq 2.00$ but were not already known to be giants (as of 2012; Riedel 2012).
4. Giants: Stars known to be giants according to the General Catalog of Variable Stars (Samus et al. 2012; in VizieR as b/GCVS), the Catalog of Galactic Carbon Stars (Alksnis et al. 2001), or SIMBAD.
5. Flyers: Stars from Region 4 of the color-color boxes, the older boxes, or spuriously identified by eye.

Proper motions from the survey ranged from $0''.000$ to $0''.397 \text{ yr}^{-1}$; additional targets found by eye were found to be moving as fast as $0''.444 \text{ yr}^{-1}$. Overall, 1016 of the stars found in the survey were moving slower than $0''.18 \text{ yr}^{-1}$.

In practice, all but one of the flagged stars in the “Probable” group were revealed to be giants after a literature search or low-resolution spectroscopy (Section 4.3). The one potential nearby star is SCR 1931-1757 (19:31:39.88–17:57:36.0, $\mu = 0.028$, P.A. = $188^\circ 2$), a spectroscopically confirmed M2.0Ve star with all 11 valid plate relations and $R_1 - R_2 = -3.03$ (SuperCOSMOS colors are apparently erroneous); its predicted distance was too far (17.67 pc by the average of 12 CCD distance estimates) to earn astrometric follow-up (Section 4).

4. Follow-up Observations

Given limited observing resources, it was decided to define a higher-priority sample of stars for follow-up. This sample included the 115 tiny proper-motion ($< 0''.18 \text{ yr}^{-1}$) candidates with an estimated distance within 15 pc that had not already been identified as giants in the literature (Regions 1, 2, and 3, if they had more than nine valid plate relations, of Figure 4), plus all 55 of the targets within 25 pc found to be X-ray bright (Section 4.1). Additional tiny proper-motion targets from the survey that were already on the observing programs were folded into our observational list, bringing it to 187 total targets of interest.

For the purpose of providing a larger selection of tiny proper-motion objects for analysis in this paper, we added an additional 12 targets from the CTIOPI program that were not found in the TINYMO survey. These additional 12 targets do not appear in the master catalog (Section 5) or discussion thereof and are marked as such in tables where they do appear. Their astrometry, photometry, and spectroscopy (where applicable) were obtained in the same way as our survey follow-up described below.

Analysis of some stars found in the TINYMO sample also appears in Riedel et al. (2014) and Riedel et al. (2017b), and objects with proper motions higher than $0''.18 \text{ yr}^{-1}$ were folded into the study published in Winters et al. (2017).

4.1. Literature Search

There are useful bodies of work in the literature that can be used to further characterize the remaining stars of interest. Apart from SIMBAD, the General Catalog of Variable Stars (Samus et al. 2012; in VizieR as b/GCVS) maintains a list of all known variable stars and can be used to identify Mira variables, carbon stars, and other semi-regular and irregular giant stars. The Catalog of Galactic Carbon Stars (Alksnis et al. 2001) also furnished some carbon star identifications. Finally, the entire list was checked against the VizieR versions of the LSPM (Lépine & Shara 2005) and NLTT (Luyten 1979) catalogs to identify previously known proper-motion objects. Identifications from these catalogs appear in the catalog (Table 5).

We searched the *ROSAT* (Voges et al. 1999, 2000) catalog for cross-matches to our objects, as giants are not generally expected to be strong X-ray emitters (I. Song 2018, private communication). Voges et al. (1999) defined the 90% limit on detections as being sources within 25'' of the optical source, with less than 25% uncertainty on the count rate; those guidelines were followed when identifying X-ray sources prioritized for photometry, spectroscopy, and astrometry. Most of these X-ray-bright objects were identified as objects of interest by Riaz et al. (2006). Because the *ROSAT* observations were carried out in the early 1990s, we applied our proper motions to move the targets back to their epoch 1991 positions using the SuperCOSMOS proper motions before carrying out the X-ray search.

4.2. Photometry

Through the existing CTIOPI program (operating since 1999 on the CTIO 0.9 m; Jao et al. 2005; Henry et al. 2006), we have obtained Johnson–Kron–Cousins *VRI* photometry (Jao et al. 2003; Winters et al. 2015) for all 187 targets. Target fields are observed in each filter on photometric nights and then transformed to Johnson–Kron–Cousins *VRI* through the use of standards from Landolt (1992, 2007). Stars were observed on at least two nights to check for consistent *VRI* photometry.

The faintest star in our sample is 2MASS 0936–2610B, with $V = 19.92$. The brightest star is the unresolved binary GJ 2122AB ($V = 9.68$), which is a well-known M1.0V star.

Accurate *VRI* photometric data increase our confidence that the candidate stars are truly nearby dwarfs because (a) the derived distance estimate uncertainties drop from 26% for the plate photometry– (and 2MASS–) based BR_2IJK relations to 15% for the CCD photometry– (and 2MASS–) based $VRIJK$ relations (Henry et al. 2004), and (b) many giants can be eliminated from the candidate pool based on photometric variability revealed by comparing their new CCD Kron–Cousins R magnitudes to existing SuperCOSMOS plate R_1 and R_2 .

The vast majority of this photometry can be found in Table 5. Photometry for all the astrometric targets reported in this paper (including the tiny proper-motion systems not found as part of the TINYMO survey) is given in Table 3.

4.3. Spectroscopy

For the stars of interest, we obtained high-S/N, low-resolution long-slit spectroscopy. The primary purpose of this spectroscopy was to identify (and remove) giant stars from our astrometric sample. The data were also intended for spectral

typing and used for measuring gravity-sensitive spectral features.

4.3.1. CTIO 1.5 m/RCSpec

Most of the spectroscopy was collected on the CTIO/SMARTS 1.5 m telescope with the Ritchie–Crétchien (RC) spectrograph using the 32/Ia first-order grating (15°13 tilt, 5994–9600 Å, $R = 500$, OG570 blocking filter) and a 2'' slit to maximize the stellar flux. The RC spectrograph uses a relatively old 1200 × 800 Loral CCD with few bad columns and no back-thinning, which minimizes fringing in the red end of the spectrum. Two distinct epochs of observations were conducted, from 2003 to 2006 for some of the additional CTIOPI targets now being presented here and from 2009 to 2011 specifically for the TINYMO survey targets. In both cases, the regular operation was two exposures of the target object, followed by one neon-argon (NeAr) lamp exposure for wavelength solution, with one flux standard taken per night.

From 2003 to 2006, observing was done in person on nine user runs. From 2009 to 2011, observing was done in SMARTS queue mode. At that time, the 32/Ia setting was no longer a common setup, so for the most part, data for TINYMO stars were also collected in single-night blocks. The flux standard was chosen by the queue manager from a small subset of stars, all of which are in IRAF's standard *onedstds* $\$iids\text{cal}/\text{ctionewcal}$ directory. Spectra were reduced using standard IRAF *onedspec*, *ccdred*, and *ctioslit* packages.

4.3.2. Lowell 1.8 m/DeVeny

Additional spectra were gathered at Lowell Observatory's Perkins 1.8 m telescope with the DeVeny spectrograph and its 400 g mm⁻¹ grating tilted at 17°, with the OG570 blocking filter, for coverage from 5800 to 9200 Å at a spectral resolution of roughly $R = 1500$. Spectra were obtained on five runs from 2009 to 2010. Owing to the observatory's northern latitude, only targets north of decl. = -36° were observed from Lowell.

The process of obtaining spectra changed considerably over the course of the project, partly owing to the fact that the DeVeny was not regularly used and rarely in the red end of the spectral range. For the first run (2009 February), only one spectrum was taken of each target and standard IRAF flux standard, with NeAr calibration lamp spectra taken at four different times throughout the night. Subsequent runs (2009 May and December) included lamps taken after each exposure and a large catalog of flat fields, and finally (2010 March and May), flat lamps were taken after every exposure. Spectra were reduced using standard IRAF *onedspec*, *ccdred*, and *kpnslit* packages.

4.3.3. CTIO 4.0 m/RCSpec

Ten objects were observed with the CTIO 4.0 m RCSpec on 2008 September 18 and 19 using the KPGLF-1 grating (632 g mm⁻¹) and an unknown blocking filter (S. Kafka 2018, private communication). The spectra are higher resolution than our CTIO 1.5 m spectra ($\Delta\lambda = 1.90 \text{ \AA}$, $R \approx 3000$) and cover 4900–8050 Å. These spectra do not have the Na I doublet or Ca II triplet used for gravity and luminosity class detection but do contain H α and the K I doublet. For some stars, this is the only spectrum available.

Table 3
Photometric Results for 26 Selected Star Systems

Name (1)	Alternate Name (2)	V_J (3)	R_{KC} (4)	I_{KC} (5)	No. of Abs. (6)	π Filter (7)	σ (8)	No. of Rel. (9)	No. of Frames (10)	J (2MASS) (11)	H (2MASS) (12)	K_s (2MASS) (13)	Spectral Type (14)	Ref ^b (15)	Phot. Dist. (16)	No. of Relations (17)	Notes (18)
NLTT 01261	DY Psc	19.88 ± 0.03	17.46 ± 0.07	15.12 ± 0.04	2	<i>I</i>	.0076	7	29	11.99 ± 0.04	11.08 ± 0.02	10.54 ± 0.02	M9.5V	(1)	11.35 ± 2.00	8	
GIC 0050	GR 50	13.97 ± 0.05	12.68 ± 0.03	11.00 ± 0.03	2	<i>R</i>	.0130	16	85	9.28 ± 0.02	8.62 ± 0.03	8.35 ± 0.02	M3.0Ve	(2)	11.73 ± 2.04	12	*
2MA 0112+1703	GU Psc	14.14 ± 0.04	13.01 ± 0.04	11.61 ± 0.03	2	<i>I</i>	.0167	7	36	10.21 ± 0.02	9.60 ± 0.02	9.35 ± 0.02	M3	(3)	31.24 ± 4.95	12	
2MA 0123-6921		19.12 ± 0.19	17.22 ± 0.04	14.91 ± 0.03	2	<i>I</i>	.0139	13	53	12.32 ± 0.02	11.71 ± 0.03	11.32 ± 0.03	M8	(4)	20.42 ± 3.22	12	
SCR 0128-1458		13.60 ± 0.04	12.33 ± 0.03	10.67 ± 0.03	3	<i>V</i>	.0099	13	70	9.06 ± 0.02	8.56 ± 0.06	8.20 ± 0.03	M3.0Ve	(2)	12.77 ± 2.00	12	*
BAR 161-012	Barta 161 12	13.42 ± 0.03	12.19 ± 0.03	10.57 ± 0.03	2	<i>R</i>	.0510	13	70	8.96 ± 0.02	8.39 ± 0.03	8.08 ± 0.03	M3.0Ve	(2)	12.34 ± 1.95	12	*
SCR 0143-0602	RBS 237	13.01 ± 0.03	11.80 ± 0.03	10.25 ± 0.03	2	<i>V</i>	.0368	12	61	8.77 ± 0.02	8.17 ± 0.03	7.91 ± 0.02	M4.0Ve	(2)	13.33 ± 2.05	12	*
SIP 0152-6329		15.41 ± 0.05	13.93 ± 0.03	12.01 ± 0.03	2	<i>R</i>	.0141	11	56	10.17 ± 0.02	9.60 ± 0.02	9.26 ± 0.02	M4.5Ve	(2)	13.69 ± 2.15	12	*
SCR 0222-6022	RBS 309	13.36 ± 0.05	12.12 ± 0.04	10.52 ± 0.04	3	<i>V</i>	.0408	11	52	8.99 ± 0.02	8.39 ± 0.04	8.10 ± 0.03	M3.0Ve	(2)	13.25 ± 2.03	12	*
2MA 0236-5203	EXO	12.06 ± 0.03	11.02 ± 0.03	9.75 ± 0.03	2	<i>V</i>	.0397	13	60	8.42 ± 0.02	7.76 ± 0.02	7.50 ± 0.03	M2.5Ve	(2)	15.61 ± 2.88	12	
2MA 0254-5108A	0235.2-5216 GSC 08057 -00342	12.08 ± 0.04	11.06 ± 0.04	9.87 ± 0.03	3	<i>V</i>	.0514	14	70	8.67 ± 0.03	8.07 ± 0.06	7.79 ± 0.03	M2.0Ve	(2)	21.45 ± 3.40	12	
2MA 0254-5108B		17.56 ± 0.06	15.95 ± 0.09	13.90 ± 0.04	3	<i>V</i>	.0458	14	70	12.07 ± 0.02	11.49 ± 0.02	11.19 ± 0.02			30.48 ± 5.94	12	
SCR 0336-2619		16.33 ± 0.04	14.76 ± 0.03	12.72 ± 0.03	2	<i>I</i>	.0117	13	68	10.68 ± 0.02	10.13 ± 0.02	9.76 ± 0.02	M4.5Ve	(2)	14.19 ± 2.21	12	*
RX 0413-0139		13.96 ± 0.03	12.66 ± 0.03	10.97 ± 0.03	2	<i>V</i>	.0345	14	58	9.38 ± 0.02	8.76 ± 0.03	8.50 ± 0.02	K5.0Ve	(2)	13.97 ± 2.17	12	
2MA 0446-1116AB	RBS 584	12.25 ± 0.05	11.05 ± 0.03	9.57 ± 0.04	2	<i>V</i>	.0162	14	71	8.14 ± 0.02	7.56 ± 0.03	7.29 ± 0.02	M4.9V	(5)	11.07 ± 1.74	12	
HD 271076		11.35 ± 0.03	10.33 ± 0.03	9.11 ± 0.03	3	<i>V</i>	.0076	9	40	7.89 ± 0.03	7.32 ± 0.03	7.05 ± 0.02	M2.0V	(2)	15.06 ± 2.32	12	*
SCR 0533-4257AB	RBS 661	12.58 ± 0.05	11.27 ± 0.04	9.59 ± 0.03	3	<i>R</i>	.0138	28	141	8.00 ± 0.03	7.40 ± 0.03	7.12 ± 0.03	M4.0VeJ	(2)	7.41 ± 1.15	12	*
LP 780-032		12.77 ± 0.03	11.55 ± 0.04	9.99 ± 0.03	3	<i>V</i>	.0111	23	111	8.51 ± 0.02	7.91 ± 0.03	7.65 ± 0.02	M4.0Ve	(2)	11.67 ± 1.80	12	
2MA 0936-2610AC		13.12 ± 0.03	11.87 ± 0.03	10.32 ± 0.03	3	<i>V</i>	.0088	9	46	8.86 ± 0.03	8.29 ± 0.05	7.96 ± 0.02	M4.0Ve	(2)	13.57 ± 2.20	12	*
2MA 0936-2610B		19.92 ± 0.29	17.46 ± 0.08	14.98 ± 0.02	2	<i>V</i>	12.27 ± 0.02	11.61 ± 0.02	11.21 ± 0.02	17.03 ± 2.73	9	*
SIP 1110-3731ABC	TWA 3ABC	12.06 ± 0.03	10.82 ± 0.03	9.20 ± 0.03	3	<i>V</i>	...	13	63	7.65 ± 0.02	7.04 ± 0.03	6.77 ± 0.02	M4.0VeJ	(2)	6.99 ± 1.07	12	*
STEPH 0164		12.75 ± 0.04	11.59 ± 0.04	10.10 ± 0.03	2	<i>V</i>	.0132	13	55	8.70 ± 0.03	8.07 ± 0.04	7.81 ± 0.03	M3.5Ve	(2)	14.23 ± 2.22	12	*
GJ 2122AB	HD 150848	9.68 ± 0.03	8.73 ± 0.03	7.69 ± 0.03	3	<i>V</i>	.0122	40	215	6.57 ± 0.02	5.94 ± 0.03	5.72 ± 0.03	M1.0V	(2)	9.81 ± 1.57	12	
UPM 1710-5300AB		11.75 ± 0.03	10.65 ± 0.03	9.31 ± 0.03	2	<i>V</i>	.0149	10	53	8.00 ± 0.03	7.41 ± 0.02	7.16 ± 0.02			13.11 ± 2.03	12	
SIP 1809-7613		15.11 ± 0.04	13.62 ± 0.03	11.71 ± 0.03	2	<i>I</i>	.0090	13	67	9.82 ± 0.02	9.28 ± 0.02	8.99 ± 0.02	M4.5Ve	(2)	12.00 ± 1.91	12	*
SCR 1816-5844		12.78 ± 0.05	11.62 ± 0.06	10.08 ± 0.04	4	<i>V</i>	.0675	15	62	8.60 ± 0.02	7.96 ± 0.06	7.70 ± 0.02	M3.5Ve	(2)	12.20 ± 1.97	12	*
DEN 1956-3207B		13.25 ± 0.03	12.01 ± 0.04	10.45 ± 0.03	2	<i>V</i>	.0196	9	45	8.96 ± 0.03	8.34 ± 0.04	8.11 ± 0.03	M4	(3)	14.18 ± 2.22	12	
DEN 1956-3207A	TYC 7443-1102-1	11.54 ± 0.03	10.64 ± 0.04	9.74 ± 0.03	2	<i>V</i>	.0307	9	45	8.71 ± 0.03	8.03 ± 0.04	7.85 ± 0.02			30.21 ± 5.14	12	
BD-13-06424		10.51 ± 0.04	9.58 ± 0.04	8.59 ± 0.03	3	<i>V</i>	.0280	15	77	7.45 ± 0.02	6.77 ± 0.04	6.57 ± 0.02	M0Ve	(6)	14.50 ± 2.67	12	

Notes. Photometry data collected on the sample. Asterisks in the notes column indicate TINYMO stars identified in the TINYMO survey itself. The *VRI* photometry and variability are original, and *JHK* is reprinted from the 2MASS Point Source Catalog (Cutri et al. 2003).

^a Astrometric results and relative photometry use new *V* filter data.

^b References: (1) Leggett et al. (2001), (2) this paper, (3) Riaz et al. (2006), (4) Schmidt et al. (2007), (5) Shkolnik et al. (2009), (6) Torres et al. (2006). “J” indicates joint spectral types from unresolved multiples.

4.3.4. CFHT/ESPaDONs

LP 780–032 was observed with ESPaDONs on CFHT on 2016 January 28. This spectrum is much higher resolution than our CTIO 1.5 m spectra and covers 3730–10290 Å at a resolving power of $R = 75000$. Spectra were processed and flat-fielded through standard methods, and barycentric velocity was removed. LP 780–032 was determined to have a radial velocity of -7 km s^{-1} and rotational velocity of 2 km s^{-1} .

4.4. Astrometry

4.4.1. CTIOPI

TINYMO targets that were spectroscopically identified as dwarfs and within 15 pc according to *VRIJHK* photometric distance estimates were placed on the CTIOPI astrometric program.

The RECONS group has been conducting the CTIOPI at the CTIO 0.9 m since 1999, until 2003 as an NOAO survey and from 2003 to the present through the SMARTS Consortium. CTIOPI uses the facility Tek #2 *VRI* filters for observations. For a period of time between 2005 and 2009, the Tek #1 *V* filter was used instead (see Subasavage et al. 2007 for more information). The filter had different astrometric (though not photometric) properties, and all results incorporating data taken in that filter are marked as such in Tables 3 and 4.

For astrometric observations, target fields are observed usually three times a year within 2 hr of transit for at least 2 yr in a single filter, chosen out of the *VRI* set to provide the optimal balance between exposure time and brightness of the reference field. Photometric frames in the appropriate filter that meet image quality and hour angle requirements may be used for astrometry. Data are reduced using the pipeline described in Jao et al. (2005) and as used in all subsequent CTIOPI publications.¹⁰

The parallax results (Table 4) indicate that 15 of the 26 systems presented here are between 25 and 50 pc away, counter to the expectations of the TINYMO selection process, while 11 systems were within the expected 25 pc.

4.4.2. FGS

One additional opportunity occurred in 2008 when the *Hubble Space Telescope*'s data bus developed a fault. As a result, the only available instruments for Cycle 16B were the fine guidance sensors (FGSs), which communicate via the telemetry subsystems.

The FGS system on *HST* can be used as an interferometer, where two of the three onboard Koesters prisms are used, with one fixed on the target, another scanning around the source to sample the interference pattern, and the third maintaining observatory pointing. The output of the interference is two S-shaped curves along orthogonal axes, from which binary stars with separations on the order of tens of milliarcseconds can be resolved by either visually identifying a second overlapping S curve or, for close-in objects, deviations from the S curves of a single star.

We took advantage of this opportunity to observe 66 stars from our X-ray-bright sample as part of HST program #11943/11944, “Binaries at the Extremes of the H–R Diagram,” PI: Douglas Gies. Roughly half of the intended list

was observed, and results of newly discovered binaries are mentioned where appropriate in Section 8.

5. The Complete Catalog (1215 Sources)

The catalog is divided into our five subsamples of descending quality, as described in Section 3.5.

1. Good targets with X-ray detections in the RASS—88 stars, of which 68 have less than $0.''18 \text{ yr}^{-1}$ (tiny) proper motion.
2. Good targets without X-ray detection—563 stars, of which 394 have tiny proper motion.
3. Probable giants ($J - K > 1.2$, $|R_1 - R_2| > 1$)—222 stars, of which all are tiny proper motion.
4. Known giants (from SIMBAD, the General Catalog of Variable Stars (Samus et al. 2012), and the Catalog of Galactic Carbon Stars (Alksnis et al. 2001))—223 stars, of which all are tiny proper motion.
5. Discarded objects not within 25 pc or the color-selection boxes. These were the “flyers,” or objects found by eye, but are included for completeness—119 stars, of which 109 are tiny proper motion.

The final catalog is presented in Table 5. All told, 114 of the stars in the catalog of 1215 targets now have published parallaxes (66 from CTIOPI efforts and 48 from van Leeuwen 2007 and Gaia Collaboration et al. 2016). Also, 251 stars have new *VRI* photometry, and 229 have new spectral types from red-optical spectra.

6. Survey Discussion

6.1. Analysis of the Photometric Cuts

Figure 5 shows the true $V - K$ colors for all targets actually observed for *VRI* photometry by CTIOPI. This displaces the targets from where they appeared in Figure 4, which was based on the simulated $v - K$ colors. It is apparent from Figure 5 that not all of our “good” (green) targets are actually dwarfs; some of them now lie in the giant locus (which is still drawn with $v - K$ color as in Figure 4). This is unsurprising, as we arrived at our “good” sample by process of elimination, and we did not have the resources to completely vet the sample.

Plotting a histogram of distance estimates from plate *BRI* and 2MASS *JHK* photometry (Figure 6) shows that the original sample was bimodal, with peaks at 25 and 1 pc. The giant-sensitive photometric cuts remove most of the stars with predicted distances less than 2 pc. As expected, all potential nearby stars with distances less than 2 pc were confirmed with spectroscopy to be giants. All of the 462 nearby low-proper-motion stars (Categories 1 and 2) can be found among the rest of the sample in the complete table described in Section 5.

6.2. Completion of TINYMO Sample

TINYMO is not complete in terms of proper motions (Figure 7), but this is not surprising, as TINYMO uses photometric cuts with no lower proper-motion limit and is not a traditional proper-motion survey. TINYMO is probing the range of proper motions more common for giants, which means we also cannot make use of reduced proper-motion diagrams that operate under the assumption that lower proper-motion objects are farther away; we are specifically looking for nearby

¹⁰ See <http://www.recons.org> for a list of publications.

Table 4
Astrometric Results for 26 Selected Star Systems

Name (1)	R.A. (J2000) (2)	Decl. (J2000) (3)	Filter (4)	N_{sea} (5)	N_{fsm} (6)	Coverage ^a (7)	Years (8)	N_{ref} (9)	$\pi(\text{Rel})$ (mas) (10)	$\pi(\text{Corr})$ (mas) (11)	$\pi(\text{Abs})$ (mas) (12)	μ (mas yr ⁻¹) (13)	P.A. (deg) (14)	V_{tan} (km s ⁻¹) (15)	Notes (16)
NLTT 01261	00 24 24.63	-01 58 20.0	<i>I</i>	7s	29	2008.70–2015.82	7.12	6	81.58 ± 2.22	0.85 ± 0.07	82.43 ± 2.22	157.1 ± 0.8	336.4 ± 0.54	9.0	
GIC 0050	00 32 53.14	-04 34 07.0	<i>R</i>	7s	85	2007.82–2015.83	8.01	7	51.89 ± 1.05	0.72 ± 0.07	52.61 ± 1.05	167.2 ± 0.5	156.4 ± 0.32	15.1	*
2MA 0112 +1703	01 12 35.06	+17 03 55.5	<i>I</i>	3s	36	2013.67–2015.96	2.29	6	18.75 ± 2.15	1.85 ± 0.18	20.60 ± 2.16	134.1 ± 2.6	135.1 ± 2.19	30.8	
2MA 0123 -6921	01 23 11.27	-69 21 38.0	<i>I</i>	7s	53	2008.70–2014.92	6.22	10	22.14 ± 1.37	0.78 ± 0.07	22.92 ± 1.37	87.4 ± 0.7	107.4 ± 0.83	18.1	
SCR 0128 -1458	01 28 39.53	-14 58 04.2	<i>V</i>	7s	70	2009.93–2015.97	6.04	5	71.84 ± 1.35	3.01 ± 0.23	74.85 ± 1.37	71.9 ± 0.8	226.0 ± 1.30	4.6	*
BAR 161-012	01 35 13.94	-07 12 51.8	<i>R</i>	6s	70	2009.94–2014.93	4.99	7	26.11 ± 1.78	1.56 ± 0.27	27.67 ± 1.80	93.3 ± 1.2	114.1 ± 1.38	16.0	*
SCR 0143 -0602	01 43 45.13	-06 02 40.1	<i>V</i>	6s	61	2009.74–2014.91	5.18	7	49.59 ± 1.48	0.93 ± 0.13	50.52 ± 1.49	47.3 ± 0.9	104.5 ± 1.96	4.4	*
SIP 0152 -6329	01 52 55.35	-63 29 30.2	<i>R</i>	8s	56	2007.82–2014.93	7.11	7	25.14 ± 1.17	1.39 ± 0.23	26.53 ± 1.19	127.0 ± 0.5	95.7 ± 0.38	22.7	*
SCR 0222 -6022	02 22 44.17	-60 22 47.6	<i>V</i>	6s	52	2009.75–2014.65	4.90	8	31.76 ± 1.66	0.94 ± 0.13	32.70 ± 1.67	126.2 ± 1.3	98.0 ± 0.92	18.3	*
2MA 0236 -5203	02 36 51.71	-52 03 03.7	<i>V</i>	6s	63	2009.92–2014.93	5.00	6	25.80 ± 1.24	1.90 ± 0.25	27.70 ± 1.26	80.4 ± 0.8	96.5 ± 0.93	13.8	
2MA 0254 -5108A	02 54 33.17	-51 08 31.4	<i>V</i>	6c	70	2009.92–2014.91	4.99	6	25.10 ± 1.64	1.95 ± 0.24	27.05 ± 1.66	85.9 ± 1.0	94.6 ± 1.04	15.0	
2MA 0254 -5108B	02 54 34.77	-51 08 28.8	<i>V</i>	6c	70	2009.92–2014.91	4.99	6	20.52 ± 2.04	1.95 ± 0.25	22.47 ± 2.06	88.2 ± 1.3	92.1 ± 1.20	18.6	
SCR 0336 -2619	03 36 31.46	-26 19 57.9	<i>I</i>	7s	68	2008.70–2015.08	6.38	9	21.12 ± 1.09	0.68 ± 0.07	21.80 ± 1.09	76.4 ± 0.5	107.9 ± 0.73	16.6	*
RX 0413 -0139	04 13 26.64	-01 39 21.2	<i>V</i>	6s	58	2009.94–2015.08	5.14	10	35.68 ± 1.90	0.74 ± 0.17	36.42 ± 1.91	127.0 ± 1.5	93.2 ± 0.99	16.5	
2MA 0446 -1116AB	04 46 51.74	-11 16 47.7	<i>V</i>	5c	71	2011.73–2016.04	4.31	8	70.77 ± 3.41	0.91 ± 0.23	71.68 ± 3.42	149.1 ± 2.1	249.2 ± 1.48	9.9	*
HD 271076	05 10 09.69	-72 36 27.9	<i>V^b</i>	5c	40	2007.81–2011.74	3.93	7	46.73 ± 2.75	2.78 ± 0.46	49.51 ± 2.79	130.7 ± 2.6	80.3 ± 1.81	12.5	*
SCR 0533 -4257AB	05 33 28.03	-42 57 20.5	<i>R</i>	9c	141	2007.81–2016.05	8.24	9	95.46 ± 1.32	0.98 ± 0.21	96.44 ± 1.34	38.8 ± 0.5	328.8 ± 1.48	1.9	*
LP 780-032	06 39 37.41	-21 01 33.3	<i>V^b</i>	8c	111	2008.70–2016.04	7.34	13	62.26 ± 0.58	1.17 ± 0.11	63.43 ± 0.59	179.2 ± 0.3	294.9 ± 0.17	13.4	*
2MA 0936 -2610AC	09 36 57.83	-26 10 11.2	<i>V</i>	4c	46	2010.16–2013.38	3.22	9	52.74 ± 1.41	1.01 ± 0.15	53.75 ± 1.42	44.1 ± 1.2	137.7 ± 2.99	3.9	*
SIP 1110 -3731AC	11 10 27.88	-37 31 52.0	<i>V</i>	6s	63	2009.32–2014.17	4.85	8	28.41 ± 3.97	0.98 ± 0.12	29.39 ± 3.97	91.8 ± 2.5	263.8 ± 2.42	14.8	*
	11 10 27.88	-37 31 52.0	<i>V</i>	6s	46	2009.32–2014.17	4.85	8	30.31 ± 6.82	0.98 ± 0.12	31.29 ± 6.82	114.6 ± 4.4	246.9 ± 4.06	17.4	*

Table 4
(Continued)

Name (1)	R.A. (J2000) (2)	Decl. (J2000) (3)	Filter (4)	N_{sea} (5)	N_{frm} (6)	Coverage ^a (7)	Years (8)	N_{ref} (9)	$\pi(\text{Rel})$ (mas) (10)	$\pi(\text{Corr})$ (mas) (11)	$\pi(\text{Abs})$ (mas) (12)	μ (mas yr ⁻¹) (13)	P.A. (deg) (14)	V_{tan} (km s ⁻¹) (15)	Notes (16)	
SIP 1110 -3731B																
STEPH 0164	12 06 22.15	-13 14 56.1	<i>V</i>	5c	55	2010.20–2014.44	4.23	5	31.63 ± 2.36	0.58 ± 0.15	32.21 ± 2.36	113.5 ± 1.7	128.7 ± 1.68	16.7	*	
GJ 2122AB	16 45 16.97	-38 48 33.3	<i>V</i> ^b	16s	215	2000.58–2016.21	15.63	8	75.69 ± 1.57	1.50 ± 0.50 ^c	77.19 ± 1.64	60.9 ± 0.4	203.8 ± 0.62	3.6		
UPM 1710 -5300AB	17 10 44.31	-53 00 25.1	<i>V</i>	5c	53	2010.50–2014.27	3.78	10	61.88 ± 2.94	2.67 ± 0.31	64.55 ± 2.96	169.1 ± 2.1	195.9 ± 1.31	12.4		
SIP 1809 -7613	18 09 06.94	-76 13 23.9	<i>I</i>	5c	67	2010.40–2014.28	3.88	10	36.12 ± 1.50	1.69 ± 0.21	37.81 ± 1.51	143.8 ± 1.2	178.2 ± 0.70	18.0	*	
SCR 1816 -5844	18 16 12.37	-58 44 05.6	<i>V</i>	6c	62	2010.50–2015.29	4.79	9	33.61 ± 1.22	0.86 ± 0.15	34.47 ± 1.23	139.8 ± 0.8	172.8 ± 0.48	19.2	*	
DEN 1956 -3207B	19 56 02.94	-32 07 18.7	<i>V</i>	4s	45	2012.83–2015.68	2.85	6	21.66 ± 1.83	1.09 ± 0.20	22.75 ± 1.84	64.1 ± 1.9	149.3 ± 3.30	13.3		
DEN 1956 -3207A	19 56 04.38	-32 07 37.7	<i>V</i>	4s	45	2012.83–2015.68	2.85	6	20.93 ± 1.77	1.09 ± 0.20	22.02 ± 1.78	62.9 ± 1.8	148.5 ± 3.24	13.5		
BD-13 -06424	23 32 30.87	-12 15 51.4	<i>V</i>	5s	77	2010.73–2015.56	4.83	5	34.19 ± 1.84	0.58 ± 0.05	34.77 ± 1.84	156.5 ± 1.6	108.7 ± 1.04	21.3		

Notes. Astrometric results derived for the sample. Asterisks in the notes column indicate TINYMO stars identified in the TINYMO survey itself.

^a “c” indicates continuous coverage, at least two epochs per observing season, and “s” indicates scattered observations, with years missing.

^b Astrometric results and relative photometry use new *V* filter data.

^c Generic correction to absolute parallax was used because the reference star field appears to be reddened by the nearby dust cloud [DB2002b] G344.85+4.27.

Table 5
TINYMO Catalog Headers

Number	Column	Unit
1	Sample Type ^a	
2	Name	
CTIOPI Astrometry		
3	R.A.	h:m:s
4	Decl.	d:m:s
5	pm	arcsec
6	P.A.	deg
7	pi	mas
8	e_pi	mas
9	r_pi	
SuperCOSMOS Photometry		
10	B_j	mag
11	R1	mag
12	R2	mag
13	I_{59F}	mag
14	Blend	
CTIOPI Photometry		
15	V	mag
16	V Blend	
17	e_V	mag
18	R	mag
19	R Blend	
20	e_R	mag
21	I	mag
22	I Blend	
23	e_I	mag
24	n_phot	
2MASS Photometry		
25	J	mag
26	J Blend	
27	e_J	mag
28	H	mag
29	H Blend	
30	e_H	mag
31	K	mag
32	K Blend	
33	e_K	mag
Spectra		
34	SpType	
35	SpType Ref	
36	ewHa	Å
37	NaI Index	
38	ewKI7699	Å
39	ewNaI	Å
Distance Estimates		
40	plate relations	
41	plate distance	pc
42	e_plate distance	pc
43	CCD relations	
44	CCD distance	pc
45	e_CCD distance	pc
HR Diagram Values		
46	Mv	mag
47	V–K	mag
48	v–K	mag

Table 5
(Continued)

Number	Column	Unit
49	J–K	mag
50	R1–R2	mag
ROSAT X-ray Data		
51	X-ray flux	cnts s ⁻¹
52	X-ray flux blend	
53	e_X ray flux	cnts s ⁻¹
54	HR1 Hardness Ratio	
55	HR1 blend	

Note. The full catalog is available electronically.

^a The samples referred to are (1) X-ray-bright stars, (2) good stars, (3) very red/probable giants, (4) known giants, and (5) discarded objects, per Section 5.

(This table is available in its entirety in machine-readable form.)

stars that move like distant giants, and as Figure 8 shows, the survey contains several such targets.

6.3. The Limit of Meaningful Proper Motion

TINYMO offers a rough idea of the point at which a proper-motion search (even if the proper motions are accurate) will be overwhelmed by giants. This limit (seen in Figure 9) appears to be around $0''.035 \text{ yr}^{-1}$, which is not coincidentally near the lower limit of Lepine’s SUPERBLINK surveys (Lepine & Gaidos 2013), $0''.04 \text{ yr}^{-1}$.

6.4. Why So Many Young Stars?

The TINYMO survey contains a large number of nearby young stars (55, counting Riedel et al. 2014, 2017a and this paper), where they make up perhaps 4% of all stars (Riedel et al. 2017b). There are two primary reasons for this. First, the TINYMO search was carried out using photometric distance estimates, which assumed every star was a single main-sequence star. Pre-main-sequence M dwarfs are brighter and therefore appear closer when estimating distances photometrically, and thus preferentially appear in the sample. Second, the space velocities of nearby stars are clustered around the local standard of rest (Figure 10) because they are still largely following the paths of the gas clouds from which they formed, and the velocity of the local standard of rest falls below $0''.18 \text{ yr}^{-1}$ beyond 21 pc (Figure 11).

The velocity peak at $15\text{--}20 \text{ km s}^{-1}$ is only partially a result of the $0''.18 \text{ yr}^{-1}$ proper-motion limit. While it is true that stars moving at $0''.18 \text{ yr}^{-1}$ could have at most 21 km s^{-1} tangential velocities if they were within 25 pc, nearly half of the sample of low-proper-motion stars was not within 25 pc, and thus the V_{tan} was not constrained to 21 km s^{-1} .

6.5. Close Passes to the Solar System

Without radial velocities, it is difficult to determine which, if any, of our objects have made close passes to the solar system. As an educated guess, however, we can take the stars with the lowest V_{tan} velocities as being the most likely to have purely radial motion. The most obvious contender is SCR 0613–2742AB, the β Pic member published in Malo et al. (2013) and Riedel et al. (2014). It does have a published radial velocity ($+22.54 \pm 1.16 \text{ km s}^{-1}$; Riedel et al. 2014), which

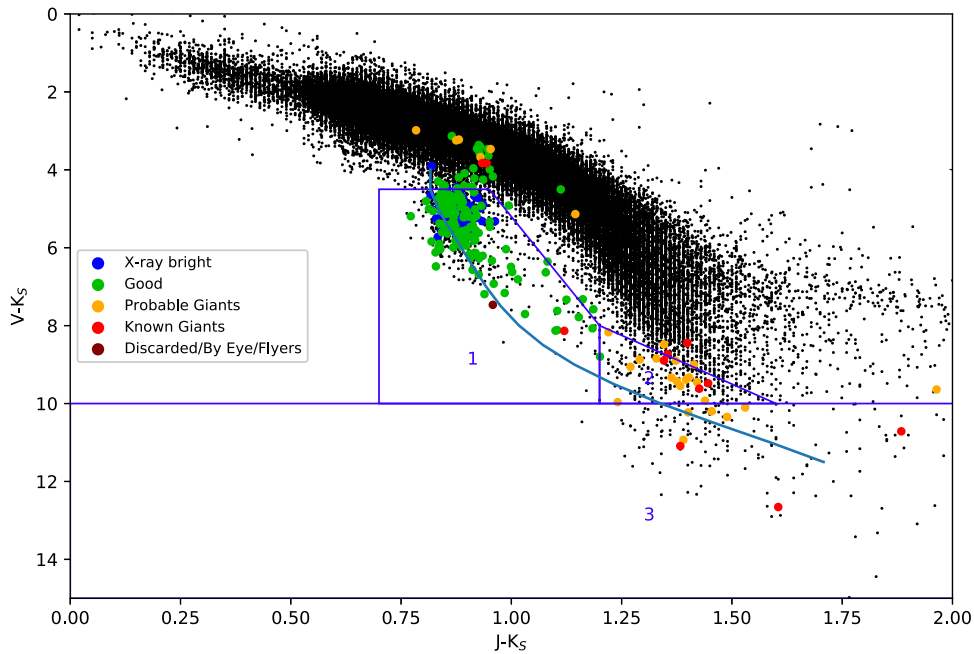


Figure 5. Final state of the TINYMO sample’s subset of stars observed for CCD photometry, plotted on top of the 88,586 stars from the photometric distance cut from Figure 4 (black points still use simulated $v-K$) for comparison. There has been some vertical shifting in the plotted positions of our photometric sample due to the differences between our simulated v and actual Johnson V . Of the stars with CCD photometry, 163 are low proper motion ($<0''.18 \text{ yr}^{-1}$), and the remaining 103 stars are high-proper-motion stars observed for other reasons (other CTIOPI targets recovered by TINYMO).

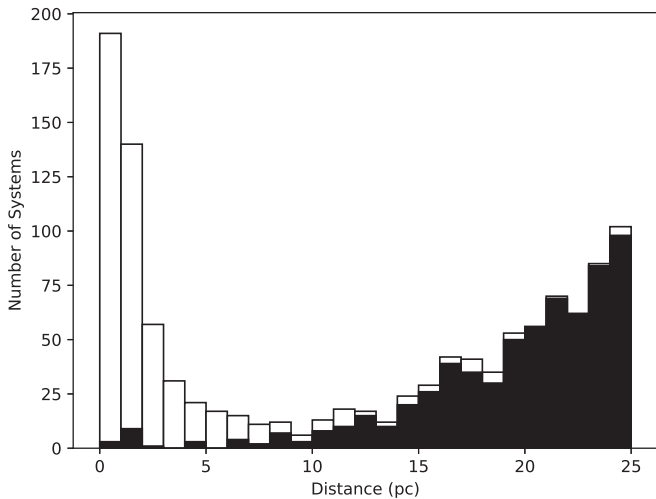


Figure 6. Plate photometric distances for (white) the entire sample of 1215 objects (including later additions found by eye) and (black) the X-ray-bright and good candidate samples. The trend of photometric distances is clearly bimodal, although applying our additional photometric cuts has weeded out an immense number of giants that only appeared to be nearby.

places its closest approach to the solar system (using an epicyclic approximation to Galactic motion; Riedel et al. 2017b) as 1.2 Myr ago at a distance of 6.1 pc. SCR 0533–4257 may be a more likely target, but without a radial velocity, it is hard to identify.

Bobylev (2010) listed no fewer than six stars predicted (via a more rigorous Galactic potential analysis) to come closer than SCR 0613–2742AB: GJ 710 (0.21 pc), GJ 551 = Proxima Centauri (0.89 pc), GJ 559A = α Centauri A (0.91 pc), GJ 559B = α Centauri B (0.91 pc), GJ 445 (1.06 pc), and GJ 699 = Barnard’s Star (1.15 pc). Of those stars, the most remarkable is GJ 710, with proper-motion vectors ($\mu_{R.A.} =$

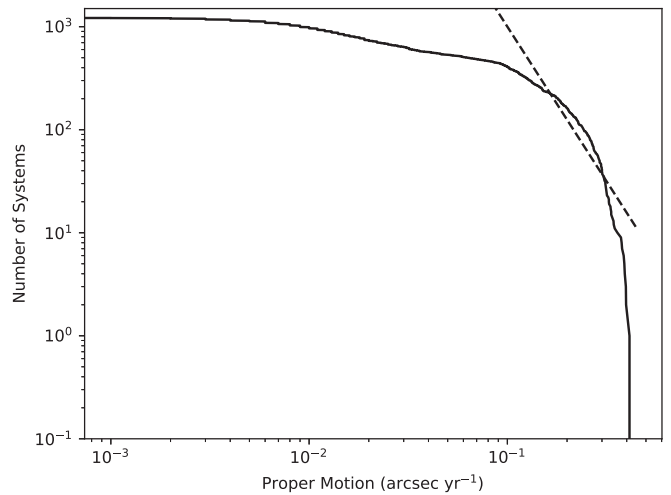


Figure 7. Diagram of the completeness of stars, as in Figure 1 of Lépine et al. (2005). The μ^{-3} curve (dotted line) follows from the assumption that the number density of stars varies as $n \propto d^3$ and proper motion varies as $\mu \propto d^{-1}$. The TINYMO sample is not complete for its proper motions.

$1.15 \pm 1.66 \text{ mas yr}^{-1}$, $\mu_{\text{decl.}} = 1.99 \pm 1.22 \text{ mas yr}^{-1}$), far smaller than any stars in the TINYMO survey.

7. Results

7.1. Nearby Stars

Although the majority of the stars followed up by the TINYMO survey were not within the 15 pc limit for which they were selected, there are 11 new stars within 25 pc in this sample. Most notable among them are SCR 0533–4257AB, a binary almost within 10 pc of the Sun, and HD 271076, which sits in front of the Large Magellanic Cloud and was at one time mistaken for a supergiant member of that satellite galaxy. More

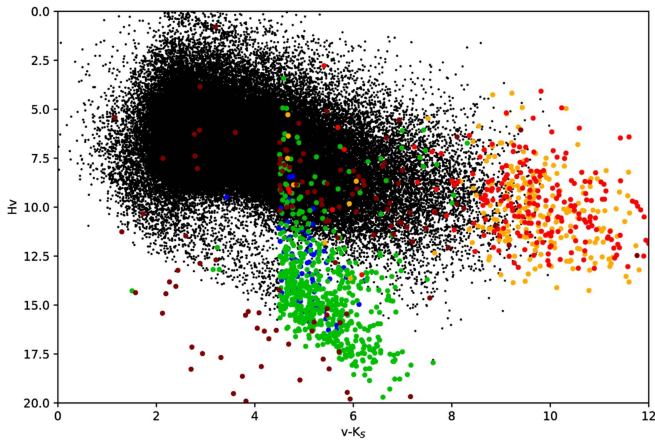


Figure 8. Reduced proper-motion diagram for the TINYMO sample, where the subsamples are colorized in the same manner as in Figure 5. Reduced proper motion (H) is $H - v = 5 \log(\frac{\pi}{\mu}) - 5$ (i.e., μ replaces π in the distance modulus equation). As can be seen above, there are clearly two loci, one (top) for giants and one (bottom) for dwarfs; while most of the green/blue “good” sample of stars obeys those trends, there are clearly green/blue “good” stars in the giant locus.

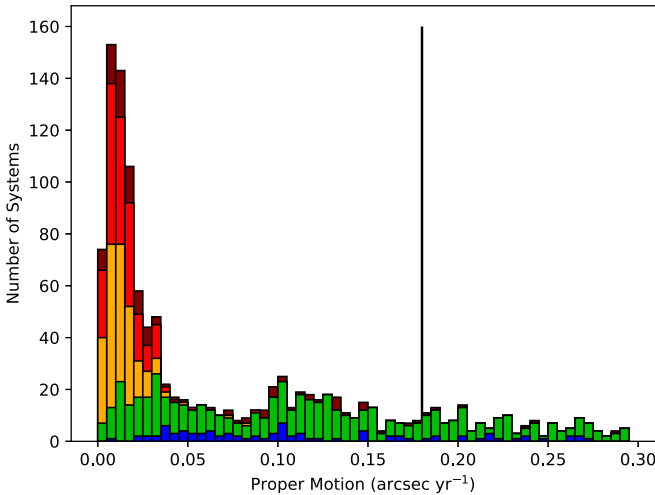


Figure 9. Proper motions of the entire survey (including all higher-proper-motion stars discovered within) in 0.005 yr^{-1} bins. Color follows Figure 5. Below 0.035 yr^{-1} , the sample is dominated by giants and suspected giants, while above that, it is dominated by X-ray-bright and regular stars. The vertical line is at 0.18 yr^{-1} and divides the TINYMO and higher-proper-motion targets found in the survey.

details of these two stars, as well as other highlighted nearby stars, are given in Section 8.

7.2. Spectral Types

Initial classification was done by eye using the techniques from Boeshaar (1976), Keenan & McNeil (1976), Kirkpatrick et al. (1991), and Henry et al. (2002), which solely focused on identifying dwarfs and giants by Na I, Ca II, and K I line features. Many giants were identified this way, as well as two carbon stars. Stars confirmed as dwarfs were placed on the CTIOPI astrometric observing program.

Spectral types (given in Table 3) were determined using the MATCHSTAR code (Riedel et al. 2014), a template-matching code that operates by comparing input red-optical spectra to a series of spectral standard-star spectra (Kirkpatrick et al. 1991; Henry et al. 1994). The code selects the portions of the

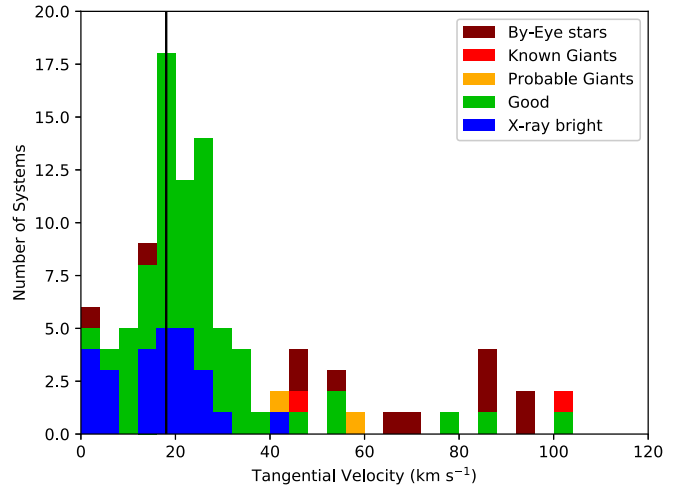


Figure 10. Tangential velocity distribution for the stars in the TINYMO sample with parallaxes. Despite having no overall constraint on V_{tan} , the distribution peaks at $15\text{--}20 \text{ km s}^{-1}$, near the local standard of rest (vertical black line).

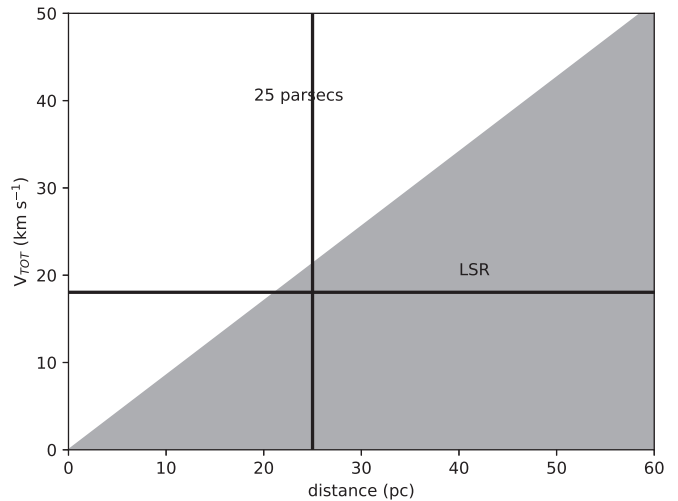


Figure 11. Objects whose distance and tangential velocity fall within the white region will move more than 0.18 yr^{-1} ; stars within the gray region will have lower proper motions. Stars moving at the velocity of the local standard of rest (18 km s^{-1}) move slower than 0.18 yr^{-1} if they are more than 21.1 pc away.

spectrum held in common between both target and standard star, masks out the atmospheric bands and $H\alpha$ emission line, divides the spectra by the templates, and takes the lowest standard deviation of a match as the correct spectral type. In this way, the code is able to type K0–K9 stars in whole types and M0.0–M9.0 in half types with a 0.5 spectral type uncertainty, as determined from fitting spectra of stars taken on different dates and with different instruments.

The code also measures, through simple numerical integration, the $H\alpha$ line equivalent width at 6563 \AA , the K I doublet line at 7699 \AA (the 7665 \AA line is masked out as part of the atmospheric A band), and the Lyo et al. (2004) Na I 8200 \AA doublet index. Emission is reported as negative equivalent widths.

7.3. They Might Be Giants

Table 6 contains a list of the new giants (confirmed by spectroscopy) discovered in the TINYMO search, a list distinct from the stars described in Tables 3 and 4. The spectral types

Table 6
New Giants and Supergiants in the TINYMO Sample

Name (1)	R.A. (2)	Decl. (3)	SpType ^a (4)
HD 270965	05 00 40.38	-71 57 52.9	K7.0var ^b
SCR 0659-5954	06 59 10.94	-59 54 58.6	M6.5var, ^c e
SCR 0703-3507	07 03 49.64	-35 07 44.3	M6.5
SCR 0705-3534	07 05 47.36	-35 34 25.8	M6.5
SCR 0711-3600	07 11 03.53	-36 00 59.7	CARBON
SCR 0747-5412	07 47 14.27	-54 12 02.5	CARBON
SCR 0747-6355	07 47 25.60	-63 55 42.3	K7.0
SCR 0749-6502	07 49 05.69	-65 02 40.0	K8.0
SCR 0753-5150	07 53 24.57	-51 50 22.0	M9.0
SCR 0753-6641	07 53 49.77	-66 41 38.3	K9.0
SCR 0805-0743	08 05 52.81	-07 43 05.7	M9.0
STEPH 0097	08 14 24.82	-13 02 22.6	M6.5
SCR 0833-6107	08 33 27.67	-61 07 58.4	M4.5var ^b
SCR 0857-6734	08 57 38.21	-67 34 10.5	M5.0
IRA 08583-2531	09 00 32.06	-25 43 14.1	M8.0
SCR 0902-7823	09 02 35.97	-78 23 14.7	M7.5
SCR 0910-7214	09 10 57.71	-72 14 52.9	M5.0
SCR 0927-8105	09 27 04.18	-81 05 00.7	M4.5var, ^c e
SCR 0932-2806	09 32 03.32	-28 06 27.0	M9.0
SCR 0938-3748	09 38 20.24	-37 48 44.6	M6.5
SCR 0945-3430	09 45 43.54	-34 30 18.1	M4.5var ^c
SCR 1044-7543	10 44 06.77	-75 43 42.2	M2.5
SCR 1044-4330	10 44 40.73	-43 30 44.2	M6.5
SCR 1048-7739	10 48 26.67	-77 39 19.1	M0.0
SCR 1058-4218	10 58 44.39	-42 18 12.3	M6.5
SCR 1111-4856	11 11 28.25	-48 56 14.3	M2.5
SCR 1138-4338	11 38 13.34	-43 38 04.6	M9.0
SCR 1228-4949	12 28 06.16	-49 49 34.5	M5.0
STEPH 0172	12 34 41.61	-00 14 14.1	M9.0
SCR 1306-4745	13 06 42.81	-47 45 25.7	M6.5var ^c
SCR 1316-5206	13 16 42.18	-52 06 38.3	M6.5
SCR 1317-4643	13 17 56.50	-46 43 54.0	M9.0var ^d
SCR 1321-4913	13 21 31.72	-49 13 09.6	M7.5
SCR 1349-7417	13 49 16.98	-74 17 15.4	M9.0
SCR 1358-4910	13 58 43.58	-49 10 52.0	M7.0
SCR 1408-3506	14 08 36.51	-35 06 02.3	M6.5
SCR 1424-4427	14 24 36.78	-44 27 05.6	M7.5
SCR 1427-4731	14 27 43.90	-47 31 13.2	M4.0
SCR 1431-4823	14 31 28.46	-48 23 12.1	M7.0
SCR 1439-4506	14 39 33.26	-45 06 42.3	M4.5
SCR 1440-7837	14 40 37.43	-78 37 11.4	K8.0
SCR 1458-4102	14 58 23.80	-41 02 27.9	M7.0var ^e
CD-81-00572	15 32 44.68	-81 43 53.0	K8.0
SCR 1534-7237	15 34 02.51	-72 37 11.1	M6.5
SCR 1544-1805	15 44 44.97	-18 05 07.1	M9.0
SCR 1551-8047	15 51 10.25	-80 47 51.5	M3.0
STEPH 0257	15 58 20.04	-06 03 37.4	M7.0
SCR 1604-7009	16 04 23.14	-70 09 03.1	M5.0
SCR 1612-6858	16 12 30.09	-68 58 52.7	M6.5
SCR 1621-6843	16 21 18.53	-68 43 58.4	M6.5
SCR 1647-6436	16 47 48.35	-64 36 43.6	M5.0
SCR 1654-0055	16 54 08.17	-00 55 04.9	M9.0
SCR 1658-6350	16 58 12.94	-63 50 49.3	M7.5
SCR 1706-6426	17 06 39.02	-64 26 23.3	M7.5var ^c
SCR 1719-6151	17 19 09.42	-61 51 55.7	M9.0
SCR 1738-6844	17 38 14.51	-68 44 52.8	M5.0var ^c
SCR 1743-4959	17 43 35.28	-49 59 10.6	M9.0
SCR 1803-7807	18 03 30.88	-78 07 21.7	M4.5
SCR 1807-5839	18 07 22.90	-58 39 59.9	M4.5
SCR 1919-2943	19 19 23.11	-29 43 15.0	M9.0
CD-35-13495	19 27 08.18	-35 15 09.6	M7.5
SCR 1943-0138	19 43 43.06	-01 38 31.6	M6.5
SCR 1944-3414	19 44 45.52	-34 14 41.2	M9.0

Table 6
(Continued)

Name (1)	R.A. (2)	Decl. (3)	SpType ^a (4)
CD-45-13476	19 53 08.97	-45 15 15.5	M7.5
SCR 1959-1639	19 59 35.79	-16 39 20.3	M8.0
SCR 2000-0837	20 00 58.33	-08 37 27.5	M9.0e
SCR 2024-2500	20 24 15.40	-25 00 56.8	M6.5
SCR 2038-0409	20 38 45.49	-04 09 27.0	M5.0
SCR 2107-5734	21 07 58.01	-57 34 17.5	M7.0var ^d
SCR 2138-4308	21 38 15.11	-43 08 40.6	M6.5var ^f
CD-24-17228	22 34 29.69	-24 15 17.7	M6.5
SCR 2305-3054	23 05 14.88	-30 54 37.1	M5.0var ^g

Notes.

^a Spectral types are derived from comparisons to dwarfs and may not be accurate. ‘e’ indicates that H α was found in emission in the spectra.

^b Variable status inferred from >1 mag R2 and R_{kc} magnitude mismatch.

^c Variable status inferred from >1 mag R1 and R2 plate magnitude mismatch.

^d Variable status inferred from >1 mag R1 and R_{kc} magnitude mismatch.

^e R_{kc} filter variability 0.18 mag.

^f R_{kc} filter variability 0.31 mag.

^g R_{kc} filter variability 0.54 mag.

given in the table were assigned by matching to M-dwarf spectra and identified as giants by Na I index measures of less than 1.02. Accordingly, not much stock should be placed in the actual spectral types of the giants in Table 6, as M-dwarf types do not correspond directly to giant or supergiant classifications; we also do not provide luminosity classes. The H α emission (denoted by ‘e’ in Table 6) reported for three stars does appear to be genuine. Samus et al. (2012) mentioned ‘characteristic late-type emission spectra’ in their description of Mira variables, which implies that this is a known phenomenon in at least Mira-type giants.

This sample contains 13 new large-amplitude photometric variables (denoted by ‘var’ in Table 6) based on either much larger than typical uncertainties on their CCD photometry (>0.1 mag mean uncertainty, which matches that of known Miras observed by CTIOPI) or >1 mag discrepancy between their R magnitudes (SuperCOSMOS and our CCD photometry). These may be Mira variables, but we lack sufficient evidence of periodicity or the required 2.5 mag amplitude for the formal definition of Miras. Photometry and other details for these stars can be found in Table 5.

7.4. Carbon Stars

Three carbon stars were observed during data collection. One, IY Hya, was observed as a comparison object; the other two are new discoveries. Figure 12 shows the spectra of the new stars and a normal M giant for comparison. Based on comparisons with spectra in Turnshek et al. (1985), they appear to be genuine C-type stars with CN bands at 6900, 7100, 7500, 7900, and 8100 Å.

7.5. Reddened Stars

Several reddened stars were picked up in TINYMO; these mostly appear to be members of various subsets of the Sco-Cen star-forming region. The stars, BD-19-04371 (16:26:23.37-19:31:35.7), SCR 1627-1925 (16:27:14.03-19:25:46.7), and SCR 1627-1924 (16:27:14.79-19:24:16.3), are all in the

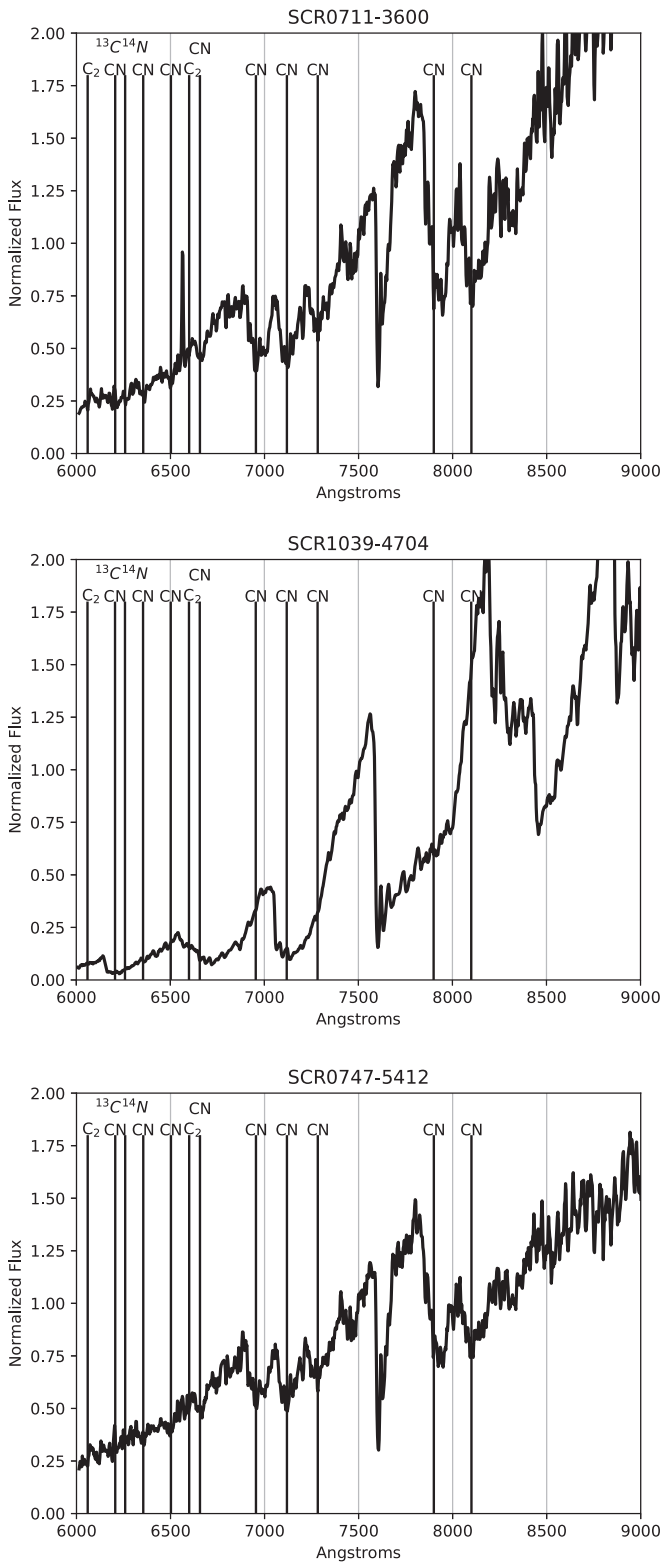


Figure 12. CTIO 1.5 m spectra of the two new carbon stars, SCR 0711–3600 (top) and SCR 0747–5412 (bottom), both from 2009 September 16, along with the approximately M7.5III giant SCR 1039–4704 (middle, from 2010 December 20) for comparison. The spectrum of a carbon star is unlike that of an M dwarf or M giant and contains unusual concentrations of carbon molecules (here CN bands known as Swan bands) rather than the typical TiO or VO bands of an M giant (compare, for instance, the spectral morphology at 7100 Å).

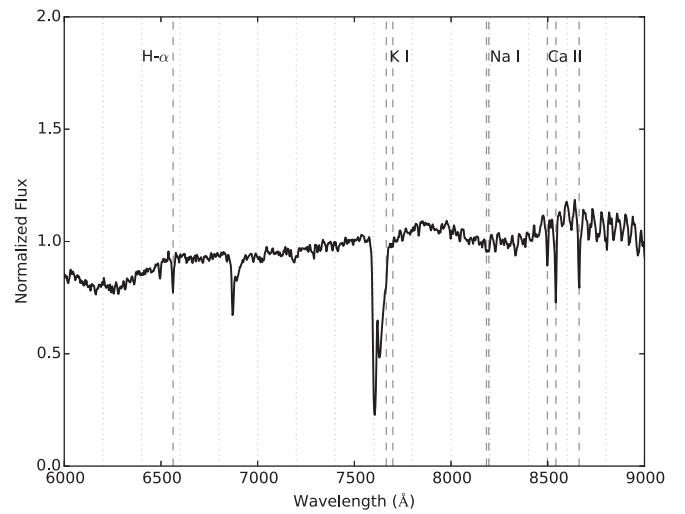


Figure 13. CTIO 1.5 m spectrum of the reddened star BD-19–04371 on 2010 September 17. The star is an apparent member of the Upper Scorpius star-forming region. Its colors are that of an M dwarf, but it is missing the strong TiO bands of M dwarfs.

region of the sky with the Upper Scorpius star-forming region, and all appear to be reddened stars of hotter spectral types (Figure 13).

A few other stars were pre-identified in SIMBAD as members of the Chamæleontis I dark cloud (CHXR11, 11:03:11.61-77:21:04.2), or ϵ Chamæleontis association. The only truly unusual set of reddened potential nearby stars were a quartet of reddened objects:

1. CD-58–07828, 20:39:19.56–58:02:29.4, $\mu = 0.036$ arcsec yr⁻¹ @ 099.3 degrees yr⁻¹,
2. CD-61–06505, 20:54:02.76–61:28:25.4, $\mu = 0.002$ arcsec yr⁻¹ @ 010.5 degrees yr⁻¹,
3. SCR 2055–6001, 20:55:43.94–60:01:46.1, $\mu = 0.018$ arcsec yr⁻¹ @ 010.4 degrees yr⁻¹,
4. SCR 2116–5825, 21:16:44.72–58:25:25.2, $\mu = 0.014$ arcsec yr⁻¹ @ 218.1 degrees yr⁻¹.

There is no known cloud in this location (as per WEBDA), which is at a high Galactic latitude. It may be that these stars are truly unrelated (their proper-motion vectors from SuperCOSMOS appear different but statistically consistent with $\mu = 0$) and all just happen to be reddened, but they are the only concentration of reddened objects that cannot be immediately explained.

7.6. New Young Stars

A substantial number of targets found in the TINYMO survey were found to be young (Figure 14, Table 7). In red spectra (6000–9000 Å), there are three useful spectroscopic features that distinguish dwarfs from giants. Ca II is strong in giants and weak in dwarfs, Na I and K I are weak in giants and strong in dwarfs, and the general principle, as outlined in Allers et al. (2007), is that neutral alkali species are stronger in dwarfs, while singly ionized species are stronger in giants. The Ca II triplet is almost completely absent in mid-M dwarfs but prominent in M giants, which makes it an easy diagnostic to use in luminosity classifying.

The Na I index is particularly useful for determining the relative surface gravities of mid- and cool M dwarfs

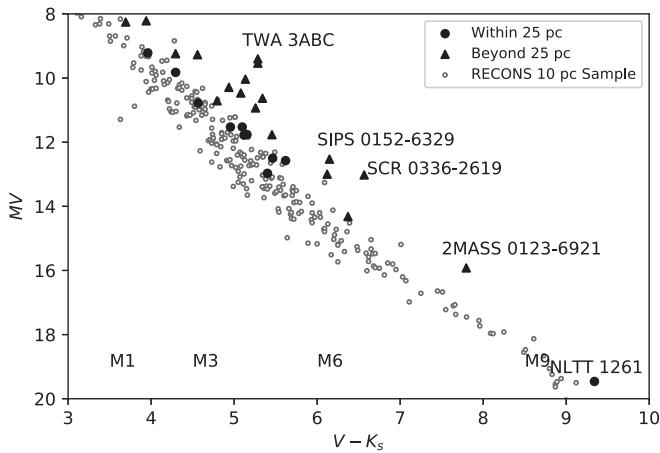


Figure 14. Color–absolute-magnitude diagram for the stars with follow-up astrometry and photometry from this paper, plotted against the RECONS 10 pc sample. A substantial number of stars lie beyond 25 pc of the Sun and are more than a magnitude overluminous compared to the mostly main-sequence stars in the RECONS 10 pc sample.

(Schlieder et al. 2012). For our purposes, we use the Lyo et al. (2004) index constructed from a 24 \AA wide region redward of the Na I 8200 \AA doublet divided by a 24 \AA wide region containing the Na I 8200 \AA doublet, as used in Murphy et al. (2010, 2013), Riedel et al. (2011), Rodriguez et al. (2013), and Riedel et al. (2014). Empirically, we have found that an index of 1.02 or less indicates a giant, and intermediate index values between dwarfs (which increase to lower temperatures) and giants (which remain flat at 1.02) indicate a low-surface-gravity pre-main-sequence star. The results for the astrometric sample of stars are shown in Figure 15.

Unfortunately, giants and dwarfs overlap at colors bluer than $V - K_s = 5$. Alkali metal lines such as Na I can also be affected by stellar activity, where emission fills in the absorption-line cores, leading to lower EWs (Reid & Hawley 1999). Slesnick et al. (2006) noted that the Na I doublet can be affected by telluric absorption over the region $8161\text{--}8282 \text{ \AA}$, leading to artificially low Na I index values for stars observed at large airmasses. Our results have large systematic errors because of this uncorrected telluric absorption.

We also use the K I 7699 \AA doublet line (though not its companion at 7665 \AA , because that portion of the spectrum is contaminated by the atmospheric A band) equivalent width as an independent indicator of surface gravity. Results in Figure 16 demonstrate again that several of the TINYMO stars are young because they lie below the envelope of field stars.

Many of the stars in this sample have $H\alpha$ in emission (see Figure 17). As noted by Zuckerman & Song (2004) and West et al. (2008), $H\alpha$ activity persists in M dwarfs for long periods of time, which means that $H\alpha$ itself is not a suitable source of youth. Strong $H\alpha$ emission has been linked to accretion and T Tauri status, but none of these stars comes close to the White & Basri (2003) limit.

The other available means for judging the youth of the stars studied here is kinematics, through which stars can be matched to nearby young moving groups (NYMGs) like β Pictoris (Song et al. 2002) and Tucana-Horologium (Zuckerman et al. 2001). The CTIOPI astrometry provides accurate values of five of the six kinematic elements (R.A., decl., $\mu_{R.A.}$, $\mu_{decl.}$, and parallax; missing only RV) necessary to fully describe a

star’s position and motion. The LACEwing code (Riedel et al. 2017b) can accommodate partial information and calculate the probability of membership in 13 NYMGs and three nearby open clusters.

LACEwing has two modes of operation: field and young star mode. In field star mode, the probabilities are calculated allowing for the possibility that the star is a field star with coincidentally similar space velocities to those of a young moving group (where field stars outnumber moving group members 50:1). In young star mode, the probabilities are calculated assuming that the star is known to be spectroscopically or photometrically young, and young field stars are evenly matched with young moving group members, 1:1. We consider LACEwing membership probabilities of 20%–50% to be low, 50%–75% to be medium, and 75%–100% to be high.

For objects with low surface gravity (below the gray lines in either Figure 15 or Figure 16), we have used LACEwing’s young star mode. For all other objects, we have used field star mode. We are accordingly biased against identifying members of AB Doradus (125 Myr) and older groups, where M-dwarf surface gravities are indistinguishable from field stars. The results of this study and spectroscopic measurements are given in Table 7.

8. System Notes

Here we describe each of the 26 systems for which parallaxes are published in this paper in Table 4. See also Table 8 for details on the various multiple systems.

(0024–0158) *NLTT 1261*—BRI 0021–0214 ($M_V = 19.46$, $V - K_s = 9.34$) has $V = 19.88$, making it the faintest star in the optical *VRI* bandpasses in this survey. Our parallax ($82.4 \pm 2.2 \text{ mas}$) is consistent with that of Tinney et al. (1995; $86.6 \pm 4.0 \text{ mas}$) and represents a factor of two improvement in the uncertainty.

(0032–0434) *GIC 50*—($M_V = 12.75$, $V - K_s = 5.62$) exhibits a perturbation due to an unseen companion spanning the full 8 yr of our data, as shown in Figure 18. A fit has been made to the data and the perturbation removed to derive the astrometry results given in Table 4. The system was resolved with *AstraLux* by Janson et al. (2014), who found it to be a triple with companions at $0''.508$ and $0''.213$.

(0112+1703) *2MA 0112+1703*—($M_V = 10.71$, $V - K_s = 4.79$) was identified by Malo et al. (2013) as a potential member of AB Dor, but the identification was less certain because the star had no measured parallax or radial velocity. While Malo et al. (2014) furnished a radial velocity, this is the first parallax. With all available information, the system is still a high-probability member of AB Dor. We do not have a spectrum of *2MA 0112+1703*, but AB Dor members are too old to distinguish from field stars by Na I or K I surface gravity, so a spectrum would not be expected to show any of the signs of youth we are looking for.

(0123–6921) *2MA 0123–6921*—($M_V = 15.92$, $V - K_s = 7.80$) is a color–magnitude diagram match (we have no spectrum to measure its $H\alpha$ or gravity features) for the TW Hydra association, but like SCR 0103–5515 and SCR 0336–2610 in Riedel et al. (2014), this system is on the wrong side of the sky from all known members. It is kinematically consistent with Tuc-Hor and to a lesser extent AB Dor but would have to be a higher-order multiple to align with other members of those groups on the HR diagram. We conclude that the system must be young and assign it to

Table 7
Youth Criteria of Parallax Targets

Name	LACEwing	Prob. (%)	Kinematic	H α	Na Index	KI EW	Youth	Note
(1)	Group	(3)	RV (km s $^{-1}$)	\AA	idx.	\AA	Flags ^a	(9)
(1)	(2)	(3)	(4)	(5)	(6)	(7)	(8)	(9)
NLTT 1261	(None)						...	
GIC 50	(None)			-1.83	1.22	2.05		*
2MA 0112+1703	AB Dor	73	-1.4 \pm 1.9				...	
2MA 0123-6921	Tuc-Hor	85	+9.9 \pm 3.4				...	
SCR 0128-1458	(None)			-3.49	1.22	2.23		*
BAR 161-012	(None)			-10.51	1.15	1.43	h N K	*
SCR 0143-0602	(None)			-5.32	1.20	1.76		*
SIPS 0152-6329	Tuc-Hor	80	+10.4 \pm 3.4	-9.72	1.19	2.52	N	*
SCR 0222-6022	Tuc-Hor	88	+11.5 \pm 3.3	-11.56	1.18	1.07	h N K	*
2MA 0236-5203	Tuc-Hor	86	+11.7 \pm 3.1	-5.53	1.09	0.54	N	
2MA 0254-5108A	Tuc-Hor	33	+12.7 \pm 3.1	-2.08	1.09	0.66		
2MA 0254-5108B	Tuc-Hor	63	+12.6 \pm 3.1				...	
SCR 0336-2619	Tuc-Hor	67	+13.5 \pm 2.6	-10.19	1.25	2.47	h N K	*
RX 0413-0139	(None)			-10.54	1.18	1.11	h N K	
2MA 0446-1116AB	(None)						...	
HD 271076	(None)			+0.20	1.11	0.82		*
SCR 0533-4257AB	(None)			-4.63	1.20	1.95		*
LP 780-032	Argus	38	+23.8 \pm 1.8	-0.26	1.21	1.69		
2MA 0936-2610AC	(None)			-2.36	1.26	2.45		*
SIPS 1110-3731AC	TW Hya	72	+12.7 \pm 2.2	-9.21	1.10	0.51	N K	*
SIPS 1110-3731B	TW Hya	62	+12.7 \pm 2.2	-9.21	1.10	0.51	N K	*
STEPH 164	(None)			-4.25	1.15	1.38		*
GJ 2122AB	(None)			+0.28	1.08	0.82		
UPM 1710-5300AB	(None)						...	
SIPS 1809-7613	β Pic	31	+6.4 \pm 2.6	-8.31	1.17	1.98	N K	*
SCR 1816-5844	Argus	69	-13.0 \pm 1.9	-6.50	1.15	1.09	N	*
DEN 1956-3207B	(None)						...	
DEN 1956-3207A	(None)						...	
BD-13-6424	β Pic	30	+0.9 \pm 1.6				...	

Notes. Youth properties are of stars in Tables 3 and 4.

^a Youth flags are “h”: H α stronger than -10 \AA ; “N”: low surface gravity by sodium index; “K”: low surface gravity by potassium EW. In all cases, these stars appears below the curves in Figures 15, 16, and 17.

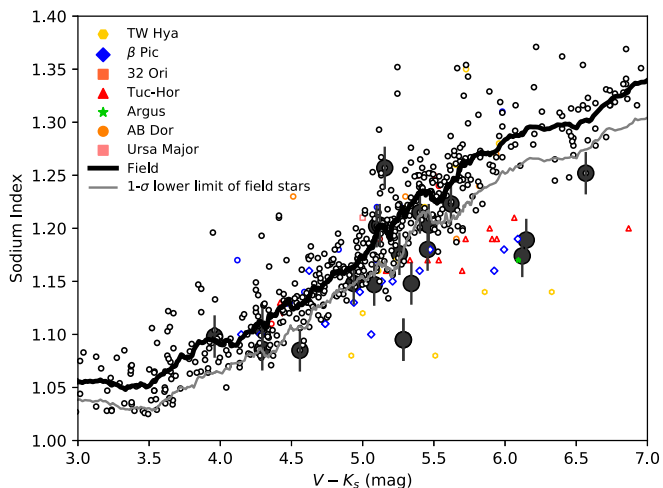


Figure 15. The Na I index from Lyo et al. (2004) vs. $V - K_s$. TINYMO objects measured spectroscopically are shown as large black points with error bars; the smaller points are young stars from Riedel et al. (2017b) and other RECONS spectral holdings measured with MATCHSTAR. A 25-point moving average (thick black line) and standard deviation (gray line) show the boundaries of inactive stars and demonstrate that many of our targets have lower surface gravities than typical field stars, though many are consistent with or even higher than the field locus.

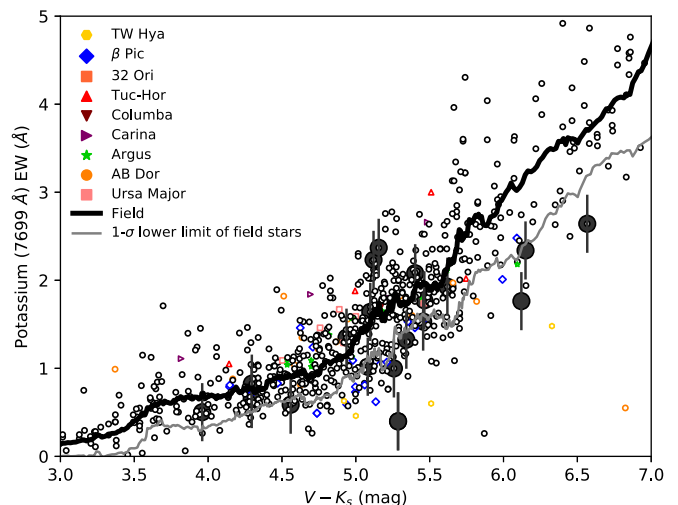


Figure 16. Same as Figure 15 but for the KI equivalent width.

Tuc-Hor; we note that it is likely to be a triple or quadruple in that case but find no evidence in our astrometric data.

(0128-1458) SCR 0128-1458—($M_V = 12.97$, $V - K_s = 5.40$) shows a possible perturbation in the 6 yr of data

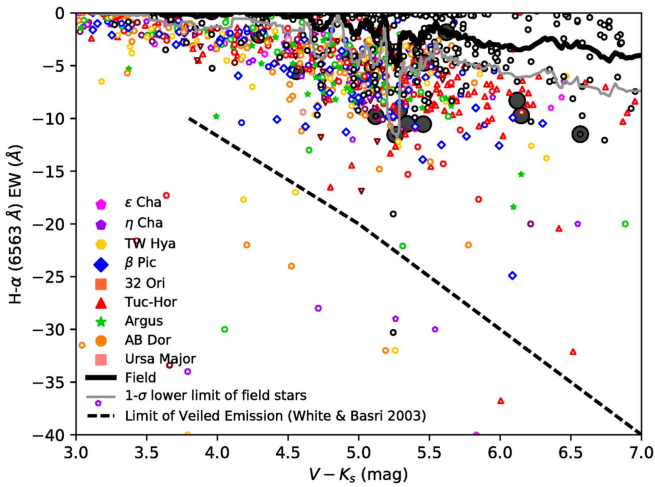


Figure 17. Same as Figure 15 but for the $H\alpha$ equivalent width and White & Basri (2003) limit (dotted black line), below which veiling from accretion is a probable concern.

available, but only in the decl. axis (Figure 19). More data are required before the companion can be confirmed. Regardless, a fit has been made to the data and the slight possible perturbation removed to derive the astrometry results given in Table 4.

(0135–0712) *BAR 161–012*—($M_V = 10.63$, $V - K_s = 5.34$) flared to a maximum of 193 mmag in R on UT 2011 October 11 and shows a variability of 51 mmag over the 5 yr data set, as shown in Figure 20. This photometric variability and a discrepancy between a photometric distance estimate of 12.3 pc and a trigonometric distance of 36.1 pc indicate that this star is likely young. While several sources, most notably Shkolnik et al. (2012), place this star in β Pic, we find that this star’s kinematics are inconsistent with any known NYMG. This star is yet another young star without membership in an NYMG.

(0143–0602) *SCR 0143–0602*—($M_V = 11.53$, $V - K_s = 5.10$) was observed to be 178 mmag in V above its baseline brightness on UT 2014 October 17, although the peak may have been higher because this offset was measured in the first frame taken that night. The star’s photometric variability (Figure 21) is 37 mmag over 5 yr, indicating that it might be young. The discrepancy between the photometric distance estimate of 13.3 pc and trigonometric distance of 19.8 pc also hints that the star might be young or, alternately, an unresolved multiple.

(0152–6329) *SIP 0152–6329*—($M_V = 12.53$, $V - K_s = 6.15$) is a new Tuc-Hor member as identified by kinematics and the sodium gravity test, with a LACEwING-derived membership probability of 80%. Gagné et al. (2015) found it to be a member of β Pic, but we find only an 11% probability of this. We do not find the star to be significantly photometrically variable in R over 7 yr.

(0222–6022) *SCR 0222–6022*—($M_V = 10.93$, $V - K_s = 5.26$) was first identified as a member of Tuc-Hor by Rodriguez et al. (2013). It is confirmed as a member based on kinematics (with 88% probability in LACEwING) and both gravity tests. The star varies by 41 mmag over 5 yr, as shown in Figure 22, supporting the premise that it is young.

(0236–5203) *2MA 0236–5203*—($M_V = 9.27$, $V - K_s = 4.56$) has a proper motion of 80 mas yr^{-1} at position angle

97° , similar to the 2MA 0254–5108AB system (discussed next) with 87 mas yr^{-1} at 93° . Zuckerman & Song (2004) identified 2MA 0236–5203 as a Tuc-Hor member, and we find it to be a member of that group via kinematics.

This star does show a photometric variability of 40 mmag, as shown in Figure 23, indicative of youth, which corroborates the low surface gravity measurement from the sodium index.

(0254–5108) *2MA 0254–5108AB*—($M_V = 9.24$, $V - K_s = 4.29(A)$, $M_V = 14.32$, $V - K_s = 6.37(B)$) is a binary with a separation of $15''.3$ at a position angle of $80^\circ.2$. We do not see any indication of orbital motion of the components in the 5 yr time span of our observations. The two components have the largest ΔV (5.48) of any resolved system under consideration here; the astrometry for the B component suffers due to its low S/N because images were taken based on the brightness of the A component. The trigonometric parallaxes differ by 1.9σ , which may be caused by the low signal on B or (alternately) taken as evidence that these are two separate members of Tuc-Hor serendipitously aligned on the sky. Assuming they are a bound system (and with the weighted mean system parallax), the A component is only marginally consistent with Tuc-Hor membership and would need to be an equal-luminosity binary to fit the Tuc-Hor isochrone. Currently, the agreement with Tuc-Hor (for both components) actually improves if the parallaxes are not combined and the two components are treated as separate star systems. The single *ROSAT* X-ray detection is likely for the A component.

Both of the stars are variable, by 51 (A) and 46 (B) mmag in V over 5 yr, although the variability for B is suspect given its low level of counts throughout the observing sequence. Component A flared to a maximum of 255 mmag above its mean value on UT 2012 July 31 (Figure 24). Both stars are almost certainly young, supported by the parallaxes that place them well above the main sequence; photometric estimates place the stars at 21 (A) and 31 (B) pc, whereas the trigonometric distances are 37 and 45 pc, respectively.

(0336–2619) *SCR 0336–2619*—($M_V = 13.02$, $V - K_s = 6.57$) is a member of Tuc-Hor, as first suggested by Gagné et al. (2015). Despite its clear spectroscopic signatures of gravity and chromospheric activity, it has an exceptionally flat light curve, shown in Figure 25.

(0413–0139) *RX 0413–0139*—($M_V = 11.77$, $V - K_s = 5.46$) exhibits photometric variability at the 35 mmag level over 5 yr, as shown in Figure 26. The astrometric residuals are poor ($\sim 9.5 \text{ mas}$) in the decl. axis due to few reference stars in the southern portion of the field.

Malo et al. (2013) reported RX 0413–0139 to be a member of the Argus association, but we find no support for that identification using our new parallax. This star and BAR 161–012 are new examples of nearby young stars without membership in any known group.

(0446–1116) *2MA 0446–1116AB*—($M_V = 11.53$, $V - K_s = 4.96$) appears elongated in our images, with two components separated by $\sim 1''.0$. This companion is too close to be properly centroided or even distinguished from the primary, which results in a parallax with a relatively high error of 3.4 mas that is unlikely to improve with additional data from our observing program.

(0510–7236) *HD 271076*—($M_V = 9.82$, $V - K_s = 4.30$) was reasonably suspected to be a supergiant in the LMC by Westerlund et al. (1981), given its location in the sky. However, at a distance of $20.2 \pm 1.1 \text{ pc}$, it is clearly a

Table 8
Multiple Star Results

Name	Binary	Type	Separation (arcsec)	Position Angle (deg)	Δ Mag. (mag)	Filter	Ref.
(1)	(2)	(3)	(4)	(5)	(6)	(7)	(8)
GIC 50	AB	VB	0.51	184		z'	Janson et al. (2014)
GIC 50	AC	VB	0.21	17		z'	Janson et al. (2014)
2MASS 0123–6921							
2MASS 0254–5103	AB	VB	15.3	80.2	5.48	V	
2MASS 0446–1116	AB	VB	~ 1.0	~ 285	~ 0.9	V	
SCR 0533–4257	AB	IB	0.056		0.7	F583W	
2MASS 0936–2610	AB	VB	41	314	3.25	K	
2MASS 0936–2610	AC	VB	0.39	284	0.5	?	(B. Mason, priv. comm.)
SIPS 1110–3731	AB	VB	~ 1.16	~ 209	~ 0.38	V	
SIPS 1110–3731	AC	SB					Webb et al. (1999)
Stephenson 164							
GJ 2122	AB	VB	0.59	255	2	V	Heintz (1987)
UPM 1710–5300	AB	VB	~ 0.77	~ 343	~ 0.69	V	
DENIS 1956–3207	AB	VB	26.37	43.9	1.71	V	

Note. Measurements are this work unless otherwise noted. AB = astrometric binary, IB = interferometric binary, SB = spectroscopic binary, VB = visual binary. Approximate measurements were determined by eye.

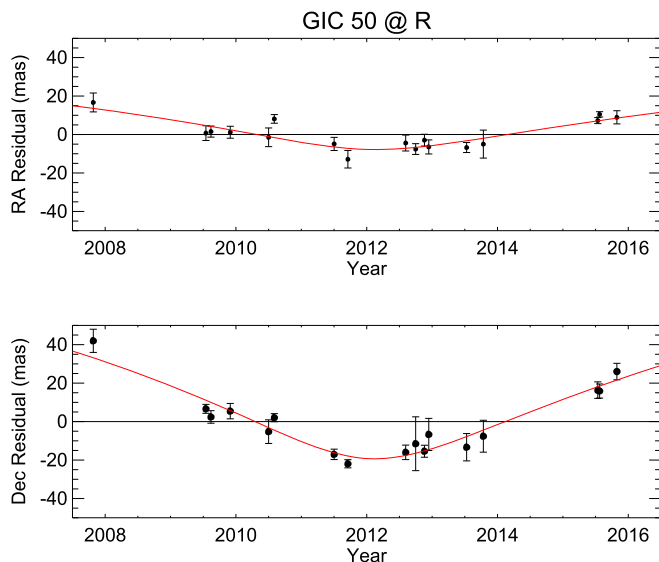


Figure 18. Perturbations in the astrometric residuals of GIC 50 (curve) due to its otherwise-unseen companion have been removed from the astrometry before the final parallax was fit.

foreground M2.0V star and a member of the solar neighborhood. Much of the error in the parallax (2.8 mas) can be attributed to a faint reference field.

(0533–4257) SCR 0533–4257AB—($M_V = 12.50$, $V - K_s = 5.46$) is the closest system in our sample, at a distance of only 10.4 ± 0.1 pc. It has a very low proper motion, only 39 mas yr^{-1} . The relatively large position angle error (1.5 deg) in Table 4 is due to this small proper motion; the proper-motion errors themselves are no worse than those for other stars in the program.

The system was identified in Riaz et al. (2006) as emitting X-rays, so we observed it during our *HST*-FGS Cycle 16B campaign. It was resolved (Figure 27) into a close binary with a 56 mas separation and $\Delta F583W = 0.7$ mag on 2008 December 2. Thus, the stars have a projected separation of roughly 0.56 au, and the system’s X-ray flux is unlikely to be due to the components’ interactions. A periodogram of our astrometric

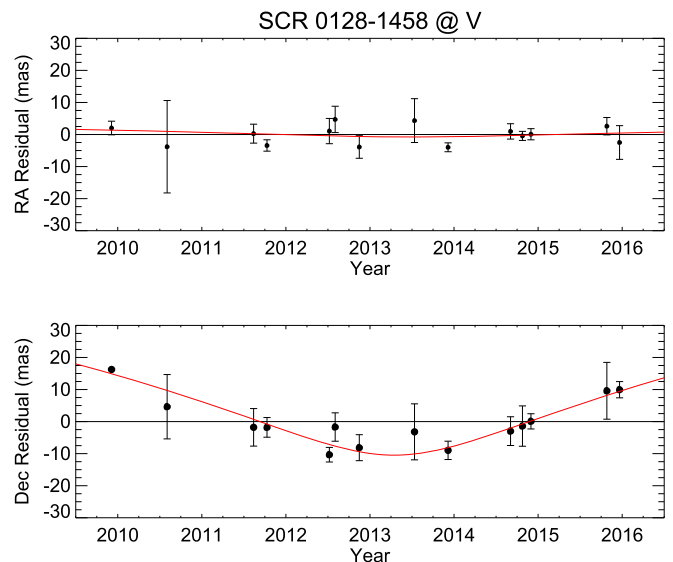


Figure 19. Same as Figure 18 but for SCR 0128–1458. There is no visible perturbation on the R.A. axis.

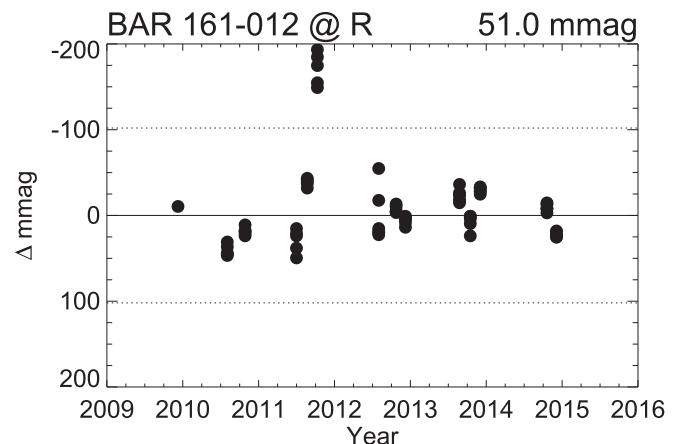


Figure 20. Relative R -band photometry of BAR 161–012 from 2009 to 2015. A flare can be seen on 2011 October 11, as well as generally high photometric variability (>20 mmag).

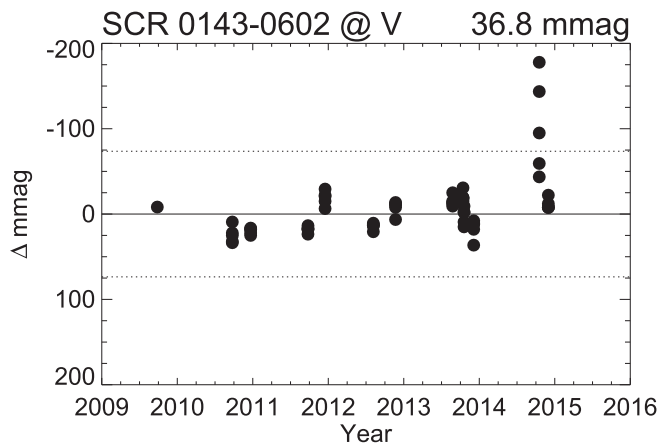


Figure 21. Same as Figure 20 but for SCR 0143–0602. A flare can be seen on UT 2014 October 17.

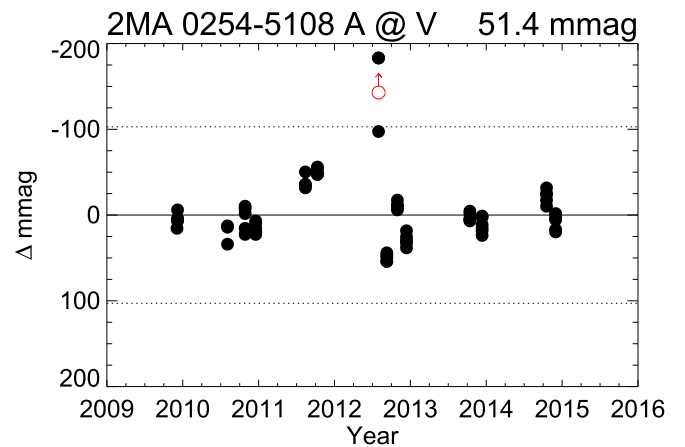


Figure 24. Same as Figure 20 but for 2MA 0254–5108A. A flare is seen on 2012 July 31. One photometric point (indicated in red) from that sequence is outside the scale of the figure.

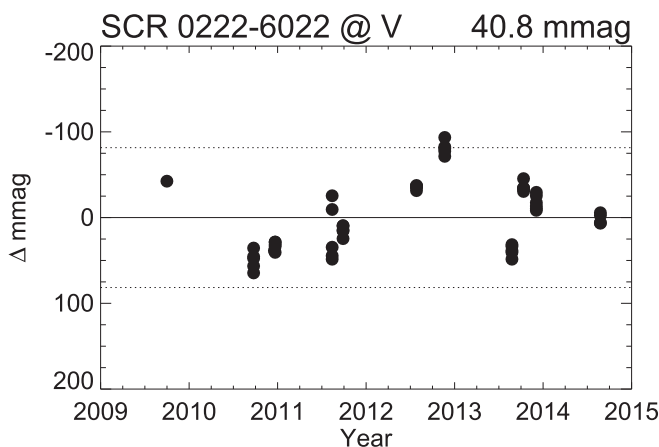


Figure 22. Same as Figure 20 but for SCR 0222–6022.

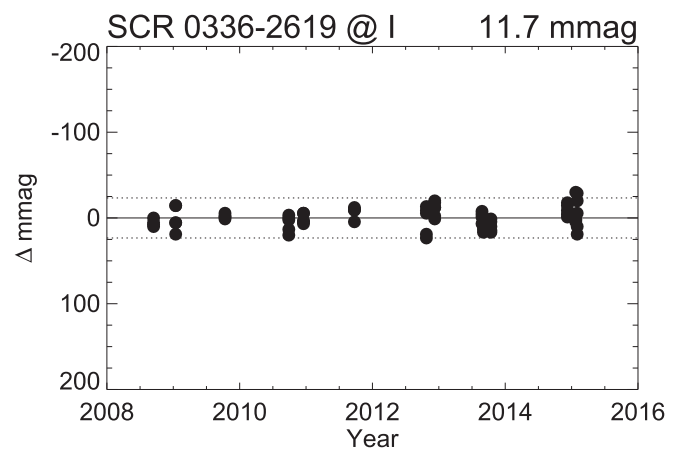


Figure 25. Same as Figure 20 but for SCR 0336–2619.

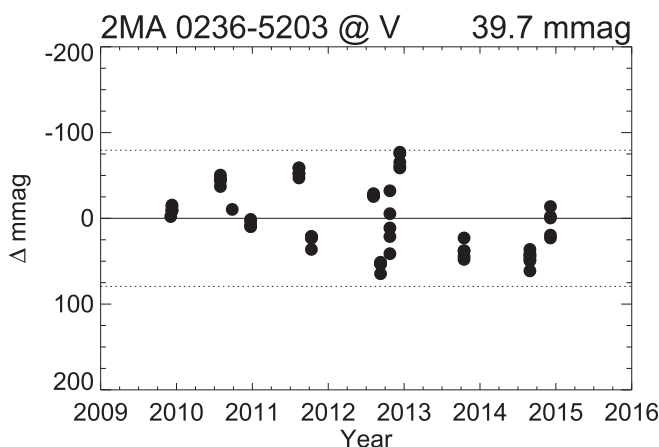


Figure 23. Same as Figure 20 but for 2MA 02362–5203.

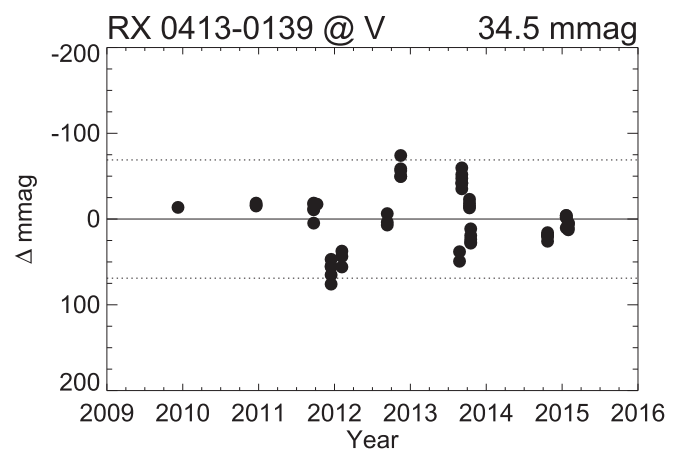


Figure 26. Same as Figure 20 but for RX 0413–0139.

data shows a peak with a period near 9 months, consistent with the projected separation for the companion in a Keplerian orbit. However, the amplitude of the perturbation is small and evident in the R.A. direction only, so we present an uncorrected parallax in Table 4.

Given the system’s X-ray emission, it is probably at least somewhat youthful, but based on its lack of low-gravity features and color–magnitude diagram position (corrected for

its multiplicity), the system is over 120 Myr old. The kinematics of the system do not place it in any of the NYMGs.

(0639–2101) *LP 780–32*—($M_V = 11.78$, $V - K_s = 5.12$) has a photometric distance estimate of 11.6 pc, which places the system closer than the parallax (15.8 pc). Kinematic analysis shows it to be a low-probability member of Argus.

(0936–2610) *2MA 0936–2610ABC*—($M_V = 11.76$, $V - K = 5.15$, $M_K = 6.61(A)$, $M_K = 9.86(B)$) is a likely common

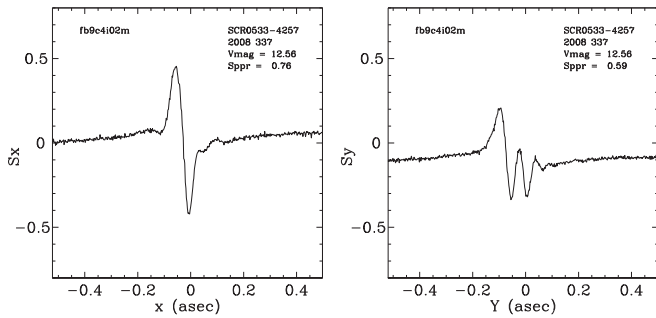


Figure 27. The X-axis (left) and Y-axis (right) *HST*-FGS preliminary results for SCR 0533–4257AB. The Y-axis “S curve” of the FGS shows a second dip to the right of the main one, revealing a companion. The companion can also be identified as a deformation in the X-axis S curve, compared to a single star, though it is not visibly apparent. Figure by Ed Nelan.

proper-motion binary separated by $41''$ at position angle 314° . While comparing images from multiple epochs (SuperCOSMOS, 2MASS, and *WISE* images) using Aladin, we discovered the possible secondary, which is not in SIMBAD. We are unable to determine a reliable proper motion or parallax for the companion using our existing data because it is 3.2 mag fainter than the primary at *K* and not exposed well enough in our images at *V* for reliable astrometry. With $VRI = 13.11, 11.86,$ and 10.31 and $JHK = 8.86, 8.29,$ and 7.96 , we estimate a photometric distance of 17.0 ± 2.7 pc for the possible companion, which is consistent with the trigonometric distance of 18.6 pc for A. The A component’s photometric distance is closer, 13.6 ± 2.2 pc. Speckle observations from 2010 (B. Mason 2018, private communication) indicate that the A component may be a close binary at $0''.39$ at 284° with a delta mag of 0.5. No sources were near the star at either the Palomar Deep Sky Survey (DSS) 1 red plate epoch (1955) or DSS2 red plate epoch (1995), making it likely that the speckle source is a comoving companion and the system as a whole is a triple.

(1110–3731) *SIP 1110–3731ABC = TWA 3ABC*—($M_V = 9.40, V - K_s = 5.29$) is one of the first known members of the TW Hya association (de la Reza et al. 1989) and has for some time been considered the closest genuine member (TWA 22AB, at 17.5 ± 0.2 pc, is now widely believed to be a member of β Pic instead; Mamajek 2005; Teixeira et al. 2009.) Webb et al. (1999) and Zuckerman & Song (2004) claimed that this system is a triple (see Table 8), where A is a spectroscopic binary, presumably SB2; with no other information given, we assume $\Delta V = \Delta K = 0$, which makes B the actual brightest component.

As shown in Figure 28, we detect two nearly equal-magnitude sources separated by $1''.16$ at a position angle of $210^\circ.2$, which implies a projected separation of 38 au. During reductions, many frames were thrown out, and most of the remaining SExtractor output had to be manually edited to correctly identify the B component. The resulting parallax precision for the two components in Table 4 is poor, with errors of 4.0 and 6.8 mas, and the measured variability is unreliable. Nevertheless, the combined weighted mean result of 33 pc is close to the expected distance to the system (42 pc) based on kinematics in Zuckerman & Song (2004). The astrometry also confirms that each star is a potential member of the TW Hya association, though only TWA 3B has a published radial velocity consistent with the predicted best-fit value.

We see minimal evidence for orbital motion in the form of different proper motions for the two components. We find the

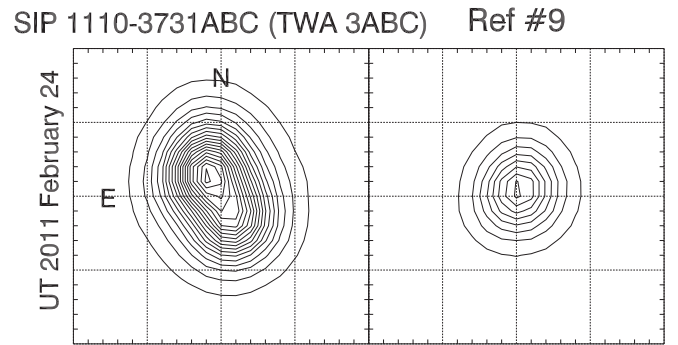


Figure 28. Positions of TWA 3 AC (NE) and B (SW) on 2011 February 24. As seen here, TWA 3B often appears as a mere elongation of the TWA 3 AC PSF, making parallax reduction difficult. Reference star #9 is shown on the right as an example single-star PSF, with the same contour intervals. Grid lines are $2''.05$ apart, or 5 pixels at the CTIO 0.9 m.

difference to be marginally significant: $\Delta\mu_{R.A.\cos\text{decl.}} = 20 \pm 11$ mas yr $^{-1}$, $\Delta\mu_{\text{decl.}} = 35 \pm 12$ mas yr $^{-1}$. The separation of the two components in our images on 2012 April 02 is $1''.16$ at position angle $210^\circ.2$, but aperture photometry for each component is not possible with our data. Instead, a point spread function (PSF) fit of the photometry data for each component is used to apply the astrometric differential color refraction (DCR) correction that is the same for both components, consistent with their similar $V - I$ colors.

(1206–1314) *STEPH 164*—($M_V = 10.29, V - K_s = 4.94$) exhibits a possible perturbation in the somewhat limited set of data we have spanning 4 yr. The discrepancy between photometric (14.2 pc) and trigonometric (31.0 pc) distance also implies that the object might be a young star and/or an unresolved multiple star. As neither kinematics nor spectroscopy identify it as a young object, we suspect that this star is a multiple-star system.

(1645–3848) *GJ 2122AB*—($M_V = 9.29, V - K_s = 3.96$) was found by Heintz (1987) to be a binary with separation $0''.59$ and an estimated by-eye delta magnitude of 2.0 (see Table 8). We see a single source in our images spanning 16 yr but find it to be an obvious astrometric binary, as shown in the nightly mean residuals of the positions after the parallax and proper-motion fit (Figure 29). Although the orbital period remains uncertain, the parallax given in Table 4 has been derived after removing our best approximation to the perturbation measured to date. Our calculated correction to absolute is an unrealistic 5.08 ± 1.34 mas because of a reddened reference field, so we have adopted a generic correction of 1.5 ± 0.5 mas and find the system to be at a distance of 12.4 pc.

The binary is also known as HIP 82021, but a bad position (off by $19''$, more than the scale of the astrometer grating) in the *Hipparcos* Input Catalog (Turon et al. 1993) leads to an enormous parallax error, and it was omitted from both official *Hipparcos* catalogs. Fabricius & Makarov (2000) rereduced the *Hipparcos* data and found a parallax of poor quality (71.3 ± 14.8 mas, 14.0 ± 2.9 pc) and again blamed the pointing error. Our parallax result (77.2 ± 2.1 mas, 13.0 ± 0.3 pc) is consistent with the Fabricius & Makarov (2000) result. (There is as yet no result from *Gaia* for this star, likely for the same reason.)

(1710–5300) *UPM 1710–5300AB*—($M_V = 10.78, V - K_s = 4.57$) is a binary for which we estimate a separation of $0''.8$ (see Table 8). The system appears as one elongated source

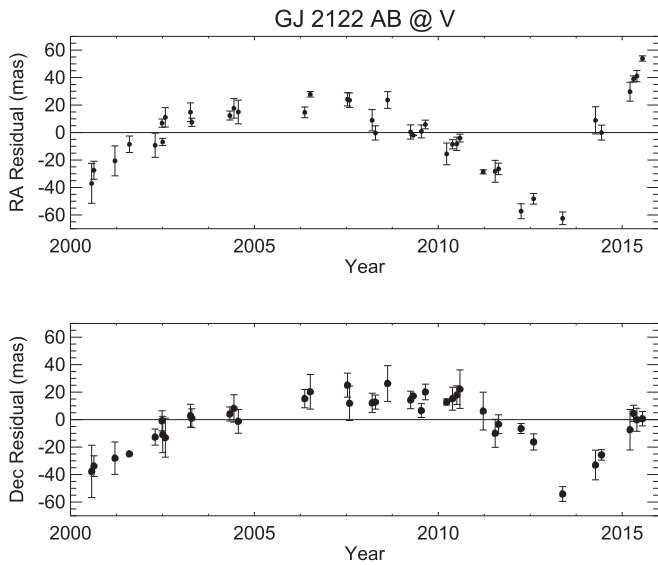


Figure 29. Same as Figure 18 but for GJ 2122AB. Large astrometric perturbations are seen in both axes.

in our data, and we determine a single parallax for the combined system with relatively high error (3.0 mas).

(1809–7613) *SIPS 1809–7613*—($M_V = 13.00$, $V - K_s = 6.12$) is a possible member of β Pictoris, as determined by a low-probability LACEwING membership of 31%, supported by low-gravity features in both sodium and potassium. The photometric variability is measured to be very low at 9 mmag, but frames were taken in the I filter, where variability is lower than in V or R .

(1816–5844) *SCR 1816–5844*—($M_V = 10.47$, $V - K_s = 5.08$) is a new member of Argus, according to kinematics, corroborated by the sodium and potassium line strengths indicative of low surface gravity. This star exhibits the highest level of photometric variability of any star reported here: 68 mmag at V over 5 yr, as shown in Figure 30. This youth indicator is supported by the discrepancy between a photometric distance of 12.2 pc and a trigonometric distance of 29.0 pc, placing the star well above the main sequence in the HR diagram.

(1956–3207) *DEN 1956–3207AB*—($M_V = 8.254$, $V - K_s = 3.69(A)$, $M_V = 10.04$, $V - K_s = 5.14(B)$) is a binary separated by $26''$ for which we determine separate but entirely consistent parallaxes placing the system at 45 pc. We do not have spectroscopy of either member of this system with which to comment on its age, but kinematic analysis with LACEwING shows no probability of membership in any known NYMG. The A component shows significant photometric variability of 31 mmag at V , while B’s variability of 20 mmag is more muted. This system does not seem to be young.

(2332–1215) *BD-13–06424*—($M_V = 8.22$, $V - K_s = 3.94$) is a known member of β Pic (Torres et al. 2006), which we confirm with our astrometric results (Table 4). We find the star to be photometrically variable at V at a level of 28 mmag during the 5 yr of data in hand.

9. Conclusions

The effort described in this paper was an experiment to determine whether or not we might reveal nearby stars via a completely photometric search, rather than via the traditional route of assuming high proper motions. The combination of

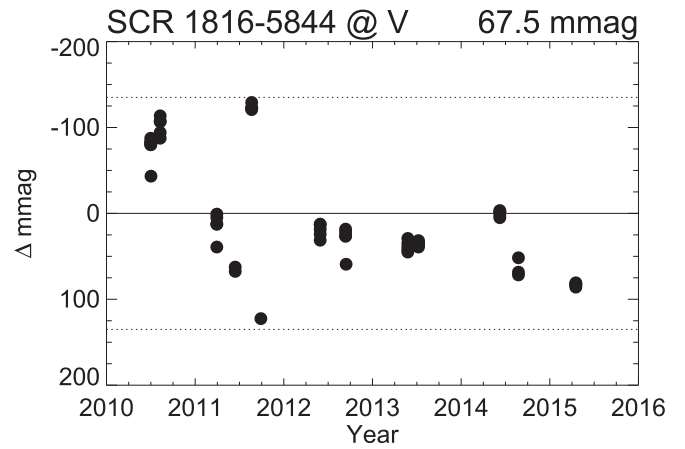


Figure 30. Same as Figure 20 but for SCR 1816–5844.

optical photometry from SuperCOSMOS and infrared photometry from 2MASS proved to be a powerful method to find nearby stars with minimal proper motions. In this paper, we report the following.

1. Twenty-nine parallaxes for 26 stellar systems, including 11 systems within 25 pc and 15 between 25 and 50 pc. The closest two systems are SCR 0533-4257AB at 10.4 pc and NLTT 1261 at 12.1 pc. All of the systems have $\mu = 38\text{--}179 \text{ mas yr}^{-1}$, which is slower moving than the 180 mas yr^{-1} threshold used by Luyten for his compendia of proper-motion stars. Thus, the experiment to find nearby, slow-moving stars was successful.
2. Fourteen pre-main-sequence stellar systems, which are identified as part of the AB Doradus (one system), Argus (two systems), Tucana-Horologium (six systems), β Pictoris (two systems), and TW Hydra (one system) moving groups. Two additional stars that do not appear to be associated with any group have been identified. The unassociated stars (along with other young nonmembers identified in Riedel et al. 2014, 2017a) hint at a complex outcome to the star formation process that yields relatively young stars that cannot be straightforwardly linked to known associations or moving groups.
3. Among those stars is LP 780–032, another possible new member of the Argus moving group at a distance of only 15 pc. This system would rank as the fifth closest young star system.

The RECONS effort has been supported by the National Science Foundation through grants AST 05-07711, AST 09-08402, and AST 14-12026. We also thank the members of the SMARTS Consortium and the CTIO staff, who enable the operations of the small telescopes at CTIO. This research has made use of results from the SAO/NASA Astrophysics Data System Bibliographic Services, as well as the SIMBAD and VizieR databases, operated at CDS, Strasbourg, France, and the Two Micron All Sky Survey, which is a joint project of the University of Massachusetts and the Infrared Processing and Analysis Center, funded by NASA and NSF. The authors would like to thank the *HST* and Lowell Observatory staff and Ed Nelan for their assistance with data collection and processing.

Facilities: CTIO:0.9m, CTIO:1.5m (RCSpec), Blanco (RCSpec), Perkins (DeVeny Spectrograph), CFHT (ESPaDONs), HST (FGS).

Software: Astropy (Astropy Collaboration et al. 2013), Numpy (Walt et al. 2011), Matplotlib (Hunter 2007), IRAF, MATCHSTAR (Riedel et al. 2014), LACEwING (Riedel et al. 2017b).

ORCID iDs

Adric R. Riedel  <https://orcid.org/0000-0003-1645-8596>
 Michele L. Silverstein  <https://orcid.org/0000-0003-2565-7909>
 Wei-Chun Jao  <https://orcid.org/0000-0003-0193-2187>
 Jennifer G. Winters  <https://orcid.org/0000-0001-6031-9513>
 John P. Subasavage  <https://orcid.org/0000-0001-5912-6191>

References

- Alksnis, A., Balklavs, A., Dzervitis, U., et al. 2001, *BaltA*, **10**, 1
- Allers, K. N., Jaffe, D. T., Luhman, K. L., et al. 2007, *ApJ*, **657**, 511
- Astropy Collaboration, Robitaille, T. P., Tollerud, E. J., et al. 2013, *A&A*, **558**, A33
- Aumer, M., & Binney, J. J. 2009, *MNRAS*, **397**, 1286
- Backman, D. E., Burgh, S. J., & Henry, T. J. 2001, in *Nearby Stars (NSTars) Workshop* (Moffet View, CA: NASA Ames Research Center), 1
- Bessel, F. W. 1838, *MNRAS*, **4**, 152
- Bessell, M. S. 1986, *PASP*, **98**, 1303
- Bobylev, V. V. 2010, *AstL*, **36**, 220
- Boeshaar, P. C. 1976, *The Spectral Classification of m-dwarf Stars* (Columbus: Ohio State Univ.)
- Boyd, M. R., Henry, T. J., Jao, W.-C., Subasavage, J. P., & Hambly, N. C. 2011a, *AJ*, **142**, 92
- Boyd, M. R., Winters, J. G., Henry, T. J., et al. 2011b, *AJ*, **142**, 10
- Gaia Collaboration, Brown, A. G. A., Vallenari, A., et al. 2016, *A&A*, **595**, A2
- Cruz, K. L., Reid, I. N., Kirkpatrick, J. D., et al. 2007, *AJ*, **133**, 439
- Cutri, R. M., Skrutskie, M. F., van Dyk, S., et al. 2003, *2MASS All Sky Catalog of Point Sources*, (NASA/IPAC Infrared Science Archive, <http://irsa.ipac.caltech.edu/applications/Gator/>)
- de la Reza, R., Torres, C. A. O., Quast, G., Castilho, B. V., & Vieira, G. L. 1989, *ApJL*, **343**, L61
- Deacon, N. R., & Hambly, N. C. 2007, *A&A*, **468**, 163
- Deacon, N. R., Hambly, N. C., & Cooke, J. A. 2005, *A&A*, **435**, 363
- Deacon, N. R., Hambly, N. C., King, R. R., & McCaughrean, M. J. 2009, *MNRAS*, **394**, 857
- Dyson, Sir F. W. 1917, *MNRAS*, **77**, 212
- Fabricius, C., & Makarov, V. V. 2000, *A&AS*, **144**, 45
- Finch, C. T., Henry, T. J., Subasavage, J. P., Jao, W., & Hambly, N. C. 2007, *AJ*, **133**, 2898
- Fitzpatrick, E. L. 1999, *PASP*, **111**, 63
- Gagné, J., Lafrenière, D., Doyon, R., Malo, L., & Artigau, É. 2015, *ApJ*, **798**, 73
- Giclas, H. L., Burnham, R., Jr., & Thomas, N. G. 1979, *LowOB*, **8**, 145
- Gizis, J. E. 1997, *AJ*, **113**, 806
- Gliese, W., & Jahreiß, H. 1991, *Preliminary Version of the Third Catalogue of Nearby Stars*, Tech. Rep. (Greenbelt, MD: NASA Goddard)
- Hambly, N. C., Davenhall, A. C., Irwin, M. J., & MacGillivray, H. T. 2001a, *MNRAS*, **326**, 1315
- Hambly, N. C., Henry, T. J., Subasavage, J. P., Brown, M. A., & Jao, W. 2004, *AJ*, **128**, 437
- Hambly, N. C., MacGillivray, H. T., Read, M. A., et al. 2001b, *MNRAS*, **326**, 1279
- Heintz, W. D. 1987, *ApJS*, **65**, 161
- Henderson, T. 1839, *MNRAS*, **4**, 168
- Henry, T. J., Jao, W., Subasavage, J. P., et al. 2006, *AJ*, **132**, 2360
- Henry, T. J., Kirkpatrick, J. D., & Simons, D. A. 1994, *AJ*, **108**, 1437
- Henry, T. J., Subasavage, J. P., Brown, M. A., et al. 2004, *AJ*, **128**, 2460
- Henry, T. J., Walkowicz, L. M., Barto, T. C., & Golimowski, D. A. 2002, *AJ*, **123**, 2002
- Høg, E., Fabricius, C., Makarov, V. V., et al. 2000, *A&A*, **355**, L27
- Hunter, J. D. 2007, *CSE*, **9**, 90
- Janson, M., Bergfors, C., Brandner, W., et al. 2014, *ApJS*, **214**, 17
- Jao, W., Henry, T. J., Subasavage, J. P., et al. 2005, *AJ*, **129**, 1954
- Jao, W.-C., Henry, T. J., Subasavage, J. P., et al. 2003, *AJ*, **125**, 332
- Keenan, P. C., & McNeil, R. C. 1976, *An Atlas of Spectra of the Cooler Stars: Types G, K, M, S, and C. Part 1: Introduction and Tables* (Columbus: Ohio State Univ. Press)
- Kirkpatrick, J. D., Henry, T. J., & McCarthy, D. W., Jr. 1991, *ApJS*, **77**, 417
- Landolt, A. U. 1992, *AJ*, **104**, 340
- Landolt, A. U. 2007, *AJ*, **133**, 2502
- Leggett, S. K., Allard, F., Geballe, T. R., Hauschildt, P. H., & Schweitzer, A. 2001, *ApJ*, **548**, 908
- Lépine, S., & Gaidos, E. 2013, *AAS Meeting 221*, 423.01
- Lépine, S., Rich, R. M., & Shara, M. M. 2005, *ApJL*, **633**, L121
- Lépine, S., & Shara, M. M. 2005, *AJ*, **129**, 1483
- Luyten, W. J. 1957, *A Catalogue of 9867 Stars in the Southern Hemisphere with Proper Motions Exceeding 0.72 Annually* (Minneapolis, MN: Lund Press)
- Luyten, W. J. 1979, *NLTT Catalogue* (Minneapolis, MN: Univ. Minnesota), 286
- Lyo, A.-R., Lawson, W. A., & Bessell, M. S. 2004, *MNRAS*, **355**, 363
- Malo, L., Artigau, É., Doyon, R., et al. 2014, *ApJ*, **788**, 81
- Malo, L., Doyon, R., Lafrenière, D., et al. 2013, *ApJ*, **762**, 88
- Mamajek, E. E. 2005, *ApJ*, **634**, 1385
- Mihalas, D., & Binney, J. 1981, *Galactic Astronomy: Structure and Kinematics* (2nd ed.; San Francisco, CA: Freeman), 608
- Murphy, S. J., Lawson, W. A., & Bessell, M. S. 2010, *MNRAS*, **406**, L50
- Murphy, S. J., Lawson, W. A., & Bessell, M. S. 2013, *MNRAS*, **435**, 1325
- Nordström, B., Mayor, M., Andersen, J., et al. 2004, *A&A*, **418**, 989
- Pokorny, R. S., Jones, H. R. A., & Hambly, N. C. 2003, *A&A*, **397**, 575
- Reid, I. N., Cruz, K. L., & Allen, P. R. 2007, *AJ*, **133**, 2825
- Reid, I. N., & Hawley, S. L. 1999, *AJ*, **117**, 343
- Riaz, B., Gizis, J. E., & Harvin, J. 2006, *AJ*, **132**, 866
- Riedel, A. R. 2012, PhD thesis, Georgia State Univ.
- Riedel, A. R., Alam, M. K., Rice, E. L., Cruz, K. L., & Henry, T. J. 2017a, *ApJ*, **840**, 87
- Riedel, A. R., Blunt, S. C., Lambrides, E. L., et al. 2017b, *AJ*, **153**, 95
- Riedel, A. R., Finch, C. T., Henry, T. J., et al. 2014, *AJ*, **147**, 85
- Riedel, A. R., Murphy, S. J., Henry, T. J., et al. 2011, *AJ*, **142**, 104
- Rodríguez, D. R., Zuckerman, B., Kastner, J. H., et al. 2013, *ApJ*, **774**, 101
- Röser, S., Schilbach, E., Piskunov, A. E., Kharchenko, N. V., & Scholz, R.-D. 2011, *A&A*, **531**, A92
- Samus, N. N., Durevich, O. V., et al. 2012, *yCat*, **1**, 2025
- Schlieder, J. E., Lépine, S., Rice, E., et al. 2012, *AJ*, **143**, 114
- Schmidt, S. J., Cruz, K. L., Bongiorno, B. J., Liebert, J., & Reid, I. N. 2007, *AJ*, **133**, 2258
- Scholz, R.-D., & Meusinger, H. 2002, *MNRAS*, **336**, L49
- Schönrich, R., Binney, J., & Dehnen, W. 2010, *MNRAS*, **403**, 1829
- Shkolnik, E., Liu, M. C., & Reid, I. N. 2009, *ApJ*, **699**, 649
- Shkolnik, E. L., Anglada-Escudé, G., Liu, M. C., et al. 2012, *ApJ*, **758**, 56
- Skuljan, J., Hearnshaw, J. B., & Cottrell, P. L. 1999, *MNRAS*, **308**, 731
- Slesnick, C. L., Carpenter, J. M., Hillenbrand, L. A., & Mamajek, E. E. 2006, *AJ*, **132**, 2665
- Song, I., Bessell, M. S., & Zuckerman, B. 2002, *ApJL*, **581**, L43
- Subasavage, J. P., Henry, T. J., Bergeron, P., et al. 2007, *AJ*, **134**, 252
- Subasavage, J. P., Henry, T. J., Hambly, N. C., et al. 2005a, *AJ*, **130**, 1658
- Subasavage, J. P., Henry, T. J., Hambly, N. C., Brown, M. A., & Jao, W. 2005b, *AJ*, **129**, 413
- Teixeira, R., Ducourant, C., Chauvin, G., et al. 2009, *A&A*, **503**, 281
- Thackeray, W. G. 1917, *MNRAS*, **77**, 204
- Tinney, C. G., Reid, I. N., Gizis, J., & Mould, J. R. 1995, *AJ*, **110**, 3014
- Torres, C. A. O., Quast, G. R., da Silva, L., et al. 2006, *A&A*, **460**, 695
- Turnshek, D. E., Turnshek, D. A., Craine, E. R., & Boeshaar, P. C. 1985, *An Atlas of Digital Spectra of Cool Stars (Types G, K, M, S and C)* (Tucson, Arizona: Western Research Company), 75
- Turon, C., Creze, M., Egret, D., et al. 1993, *BICDS*, **43**, 5
- van Leeuwen, F. (ed.) 2007, *Hipparcos the New Reduction of the Raw Data* (Berlin: Springer)
- Voges, W., Aschenbach, B., Boller, T., et al. 1999, *A&A*, **349**, 389
- Voges, W., Aschenbach, B., Boller, T., et al. 2000, *IAUC*, **7432**, 1
- Walt, S. v. d., Colbert, S. C., & Varoquaux, G. 2011, *CSE*, **13**, 22
- Webb, R. A., Zuckerman, B., Platais, I., et al. 1999, *ApJL*, **512**, L63
- West, A. A., Hawley, S. L., Bochanski, J. J., et al. 2008, *AJ*, **135**, 785
- Westerlund, B. E., Olander, N., & Hedín, B. 1981, *A&AS*, **43**, 267
- White, R. J., & Basri, G. 2003, *ApJ*, **582**, 1109
- Winters, J. G., Henry, T. J., Lurie, J. C., et al. 2015, *AJ*, **149**, 5
- Winters, J. G., Sevrinsky, R. A., Jao, W.-C., et al. 2017, *AJ*, **153**, 14
- Wroblewski, H., & Torres, C. 1989, *A&AS*, **78**, 231
- Zacharias, N., Finch, C. T., Girard, T. M., et al. 2013, *AJ*, **145**, 44
- Zuckerman, B., & Song, I. 2004, *ARA&A*, **42**, 685
- Zuckerman, B., Song, I., & Webb, R. A. 2001, *ApJ*, **559**, 388